Regional Air Quality Modeling System (RAQMS) predictions of the tropospheric ozone budget over east Asia

R. B. Pierce,[1] J. A. Al-Saadi,[1] T. Schaack,[2] A. Lenzen,[2] T. Zapotocny,[2] D. Johnson,[2]
C. Kittaka,[3,4] M. Buker,[2] M. H. Hitchman,[2] G. Tripoli,[2] T. D. Fairlie,[1] J. R. Olson,[1]
M. Natarajan,[1] J. Crawford,[1] J. Fishman,[1] M. Avery[1] E. V. Browell,[1] J. Creilson,[3,4]
Y. Kondo,[5] and S. T. Sandholm[6]

[1]   The NASA Langley Research Center and University of Wisconsin Regional Air Quality Modeling System (RAQMS) is used to estimate the tropospheric ozone budget over east Asia during the NASA Global Tropospheric Experiment (GTE) Transport and Chemical Evolution over the Pacific (TRACE-P) mission. The computed ozone budget explicitly accounts for stratosphere/troposphere exchange (STE) and in situ ozone production using on-line chemical calculations. The east Asian O_3 budget is computed during the period from 7 March to 12 April 2001. Gross formation dominates STE by a ratio of 7 to 1 in east Asia during TRACE-P. However, this ratio is strongly influenced by altitude of the tropopause. Approximately 30% of the ozone that is advected across the tropopause over east Asia is subsequently advected out over the western Pacific within the upper 4 km of the troposphere by the Japan jet. The average net photochemical production (gross formation-gross destruction) within the regional domain is 0.37 Tg d^{-1} or 7% of the average flux at the eastern boundary of the domain during the TRACE-P time period. The budget analysis shows a very close balance between sources and sinks within the RAQMS regional domain during the TRACE-P time period. This balance results in very small average accumulation ($\sim$1 Tg) of O_3 in the east Asian region and very little net export averaged over the period (0.03 Tg d^{-1}). The low ozone export from east Asia predicted by RAQMS during TRACE-P is a consequence of relatively high dry deposition rates, which are 37% of the gross ozone formation (1.469 Tg d^{-1}) within the TRACE-P regional domain.   *INDEX TERMS:* 0345 Atmospheric Composition and Structure: Pollution—urban and regional (0305); 0365 Atmospheric Composition and Structure: Troposphere—composition and chemistry; 0368 Atmospheric Composition and Structure: Troposphere—constituent transport and chemistry; 3362 Meteorology and Atmospheric Dynamics: Stratosphere/troposphere interactions; 3367 Meteorology and Atmospheric Dynamics: Theoretical modeling; *KEYWORDS:* tropospheric ozone, Asian emissions, stratosphere-troposphere exchange, ozone budget, regional photochemical modeling, global photochemical modeling

1.   Introduction

[2]   The global tropospheric ozone budget is composed of two primary sources: input from the stratosphere and in situ

photochemical generation. The relative importance of these two sources has been the focus of numerous studies throughout the past three decades [e.g., *Fishman and Crutzen*, 1978; *Fishman*, 1985; *Wang et al.*, 1998]. It is clear that there are specific times of the year and regions around the planet where one source term is dominant. For example, high levels of ozone in the upper free troposphere downwind from a region of cyclogenesis and tropopause folding are likely the result of stratosphere-troposphere exchange [e.g., *Danielsen et al.*, 1987]. Conversely, high concentrations in the planetary boundary layer where a large high pressure system has dominated the weather pattern for several days are likely the result of efficient photochemical generation of ozone from pollution. The relative importance of these sources during spring in east Asia is less clear. Quantifying the east Asian tropospheric ozone budget

---

[1]NASA Langley Research Center, Hampton, Virginia, USA.
[2]Space Science and Engineering Center, University of Wisconsin, Madison, Wisconsin, USA.
[3]Science Applications International Corporation, Hampton, Virginia, USA.
[4]Also at NASA Langley Research Center, Hampton, Virginia, USA.
[5]Center for Advanced Science and Technology, University of Tokyo, Tokyo, Japan.
[6]Center for Advanced Science and Technology, Georgia Institute of Technology, Atlanta, Georgia, USA.
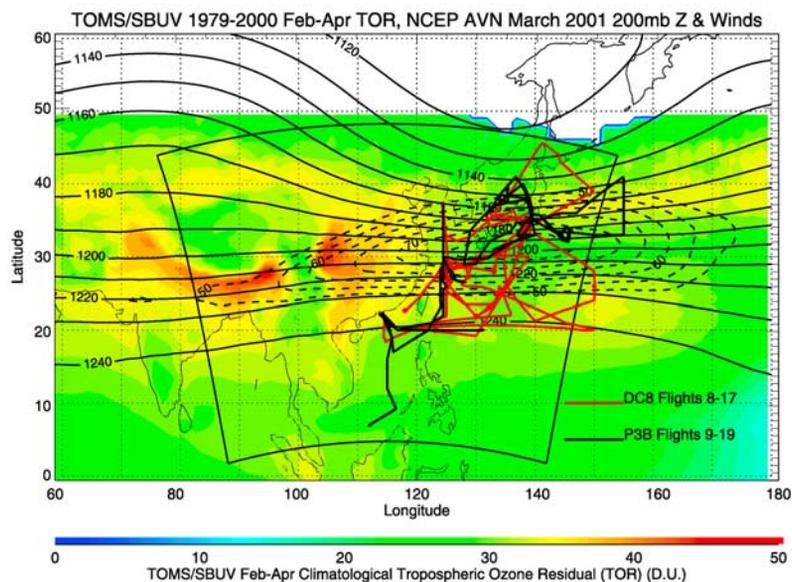
Figure 1. Climatological February–April tropospheric ozone residual (TOR) in Dobson units (colored). East Asian DC-8 (red) and P-3B (black) flights during TRACE-P, March 2001 200 mb winds (m s^{-1}) (dashed contours) and geopotential heights (dam) (solid contours).

during the spring 2001 Transport and Chemical Evolution over the Pacific (TRACE-P) mission is the focus of this study.

[3] The TRACE-P mission was conducted by the Global Tropospheric Experiment (GTE) of the National Aeronautics and Space Administration (NASA) during February–April 2001. The goals of TRACE-P included determining the chemical composition of Asian outflow, quantifying the export of chemically and radiatively important gases, determining the chemical evolution of the outflow, and understanding the processes which control its evolution [*Jacob et al.*, 2003]. TRACE-P observational goals were accomplished through an intensive measurement campaign conducted with the NASA DC-8 and P-3B aircraft and ground based instrumentation.

[4] Figure 1 shows the climatological (1979–2000) February–April tropospheric ozone residual (TOR; http://asd-www.larc.nasa.gov/TOR/data.html) derived from the difference between Total Ozone Mapping Spectrometer (TOMS) total column ozone measurements (http://toms.gsfc.nasa.gov/ozone/ozone.html) and Solar Backscatter UltraViolet (SBUV) stratospheric column measurements [*Fishman et al.*, 2003] (available at http://www.atmos-chem-phys.org/acpd/3/1). The east Asian TOR shows high tropospheric column ozone (>40 Dobson units (DU)) over the Ganges River valley and central China. This high ozone appears to be advected over the western Pacific Ocean between 35° and 40°N. The east Asian components of the DC-8 and P-3B flights during TRACE-P are indicated by bold lines in Figure 1. The flights were primarily within the East China Sea, Sea of Japan and Western Pacific. The prevailing offshore flow during this time period [*Fuelberg et al.*, 2003] indicates that the TRACE-P flights were downwind of regions with large industrial emissions, such as Shanghai, Beijing, and Seoul, and to the north of climatological biomass burning regions in Thailand, Cambodia, and Vietnam [*Duncan et al.*, 2002].

However, large quantities of ozone are also brought down from the stratosphere in this region during the spring [*Carmichael et al.*, 1998].

[5] *Carmichael et al.* [1998] used the Sulfur Transport Eulerian Model (STEM-II) regional-scale transport/chemistry model to assess the relative importance of downward transport from the upper troposphere and in situ production in determining the ozone distribution in east Asia during 1–15 May 1987. They found that high ozone levels near 1–2 km above the surface, observed in association with frontal passages, were largely determined by downward fluxes from the upper troposphere, particularly north of 30°N. In situ chemical production generally dominated below 1 km, with more than 50% of the ozone produced by anthropogenic emissions of precursors, primarily NO$_x$, over SE China, Taiwan, Korea, the Japan Sea, and central Japan.

[6] *Liu et al.* [2002] used the Goddard Earth Observing System chemical transport model (GEOS-CHEM) [*Bey et al.*, 2001a] to quantify anthropogenic and natural influences on east Asian ozone. High ozone mixing ratios observed by ozonesondes during March in the lower troposphere over Hong Kong were shown to be strongly influenced by east Asian biomass burning events. Stratospheric influences were most pronounced in the upper troposphere over Hong Kong during January–April. *Liu et al.* [2002] estimate that anthropogenic (biomass + fossil fuel) emissions from east Asia result in eastward ozone fluxes at 150°E which peak at ∼0.575 Tg d^{-1} when integrated from 10°N to 60°N during March. *Bey et al.* [2001b] used GEOS-CHEM to interpret measurements taken during the February–March 1994 GTE Pacific Exploratory Mission (PEM)-West B mission [*Hoell et al.*, 1997] and found that Asian fossil fuel + biomass burning emissions led to gross photochemical formation of 18.9 Gmol d^{-1} within the Asian boundary layer (0–3 km) with gross photochemical destruction and surface deposition of 6.4 Gmol d^{-1} and 4.2 Gmol d^{-1}, respectively.

[7] From a meteorological perspective, east Asia is a preferred region for springtime lee cyclogenesis over the Mongolian Plateau and coastal cyclogenesis in the Sea of Japan and East China Sea [*Chen et al.*, 1991]. During March 2001, synoptic storms formed within the TRACE-P domain on average every 4 days [*Fuelberg et al.*, 2003]. Consequently, transport of east Asian emissions during TRACE-P was dominated by synoptic-scale frontal lifting of polluted continental boundary layer air in the warm sector of the developing cyclones [*Jaffe et al.*, 1999; *Kaneyasu et al.*, 2000; *Bey et al.*, 2001b]. Frontal lifting is an effective means of transporting boundary layer air to the middle and upper troposphere, where strong winds can lead to long-range transport of the east Asian emissions. Tropopause folds, which can bring stratospheric air deep into the free troposphere, are also associated with rapidly developing cyclones and upper-level frontogenesis [*Lamarque and Hess*, 1994].

[8] The subtropical jet stream, with 200 mb wind speeds of greater than 75 m s^{-1} in the jet core, determines middle and upper tropospheric winds over east Asia during March (Figure 1). This jet stream, often referred to as the "Japan Jet", is located in the axis of the large-scale upper tropospheric climatological trough (Figure 1). The southern flank of this large-scale trough is a preferred region for stratosphere-troposphere exchange (STE) in the Northern Hemisphere winter [*Hoerling et al.*, 1993]. The "tropopause break", defined as a break in the altitude of the tropopause or narrow region of indistinct tropopause [*Palmen and Newton*, 1969], is located to the south of this trough, coincident with the subtropical jet stream. Isentropic surfaces between approximately 380 K and 320 K intersect the tropopause break and connect the lowermost extratropical stratosphere to the subtropical troposphere [*Holton et al.*, 1995]. Quasi-horizontal isentropic motion across the tropopause break can lead to STE [*Folkins and Appenzeller*, 1996]. *Seo and Bowman* [2001] found that globally, the largest stratosphere to troposphere fluxes occurred in Northern Hemisphere spring near 30°N off the coast of east Asia. This isentropic STE is controlled by Rossby wave breaking along the subtropical jet and is consistent with the climatology of Rossby wave breaking on the 350 K isentrope [*Postel and Hitchman*, 1999].

[9] In situ ozone production, strong STE, and rapid frontal lifting and tropopause folding due to frequent cyclogenesis result in a complex and rapidly evolving east Asian tropospheric ozone distribution during Northern Hemisphere springtime, complicating the diagnosis of an ozone budget for this region. In the current study we use the Regional Air Quality Modeling System (RAQMS), which was jointly developed by the NASA Langley Research Center (LaRC) and University of Wisconsin-Madison (UW), to estimate the ozone budget over east Asia during TRACE-P.

[10] The paper is organized as follows. Section 2 describes the RAQMS model. Section 3 presents a discussion of the method used for estimating STE during TRACE-P. Section 4 describes the RAQMS TRACE-P simulation and compares the predictions with satellite and in situ observations as well as box model estimates of ozone photochemistry to assess the fidelity of the simulations. Section 5 presents results from the STE calculations and

section 6 discusses the east Asian tropospheric ozone budget analysis. Discussion and conclusions are presented in section 7.

2. RAQMS Model Description

[11] RAQMS is a multiscale meteorological and chemical modeling system for predicting stratospheric and tropospheric chemistry. RAQMS combines two meteorological forecast models (regional domain nested within a global domain) developed at UW with a stratospheric-tropospheric chemical prediction scheme that was developed at LaRC. The nesting is one way, with chemical predictions from the global component (RAQMS$_G$) providing boundary conditions for a higher resolution nested component (RAQMS$_N$). During TRACE-P, RAQMS$_G$ was run using a 2° × 2° latitude-longitude resolution and RAQMS$_N$ was run using a rotated equidistant projection centered at 26.5°N and 115.0°E with 110 km horizontal resolution (60 grid points in east–west direction and 45 grid points in north–south direction). The TRACE-P RAQMS$_N$ domain is shown in Figure 1 and includes most of eastern and central Asia. The southern and western boundaries of the domain were chosen to include the primary biomass burning emission sources in SE Asia and the northern and eastern boundaries where chosen to capture the full extent of TRACE-P flight tracks. The RAQMS chemical predictions are conducted on-line using instantaneous meteorological conditions to accurately account for large-scale advective processes and the exchange of trace gases via moist convection and boundary layer turbulence.

[12] The RAQMS$_G$ meteorological prediction model is based on a vertical coordinate that smoothly transitions from terrain-following at the earth's surface to isentropic in the middle to upper troposphere (UW θ-η model). Numerical integration in isentropic coordinates provides decided advantages for simulation of the long-range transport of atmospheric properties [*Johnson et al.*, 1993, 2000, 2002; *Zapotocny et al.*, 1997a, 1997b]. These advantages are most pronounced in baroclinic regimes, where transport is primarily two-dimensional in isentropic coordinates and errors related to vertical advection are negligible. This simplification translates to improved simulation of atmospheric transport of conservative tracers [*Zapotocny et al.*, 1996, 1997a, 1997b]. The UW θ-η model was developed through modification of the UW hybrid isentropic-sigma (θ-σ) coordinate model [*Zapotocny et al.*, 1994, 1996, 1997a, 1997b; *Johnson et al.*, 2000, 2002] and employs flux form piecewise parabolic method (PPM) numerics [*Colella and Woodward*, 1984; *Carpenter*, 1990] on the Arakawa A grid. The PPM scheme is highly accurate both in the vicinity of sharp gradients and for smooth flows [*Carpenter*, 1990]. The monotonicity constraint employed frees the solutions from spurious oscillations, and fields such as water vapor, chemical species, and mass within isentropic layers remain positive definite during integration. The UW θ-η model incorporates the full suite of the National Center for Atmospheric Research (NCAR) Community Climate Model 3 (CCM3) physical parameterizations including radiation, moist convection, vertical diffusion, gravity wave drag, Planetary Boundary Layer (PBL) scheme, and surface fluxes. *Kiehl et al.* [1996, 1998] provide a detailed descrip-

tion of the physical parameterizations employed in CCM3. Vertical mixing due to nonlocal atmospheric boundary layer turbulence [*Holtslag and Boville*, 1993] and mass-flux convection [*Zhang and McFarlane*, 1995] are applied to the transported chemical species.

[13] The RAQMS$_N$ meteorological prediction model is the UW Nonhydrostatic Modeling System (UW-NMS) [*Tripoli*, 1992]. UW-NMS is a regional-scale nonhydrostatic numerical weather prediction model that can resolve atmospheric structure on spatial scales as low as 10 km in the horizontal and 200–400 m in the vertical. Advection is formulated using a sixth-order Crowley scheme in flux form. Unresolved turbulent exchange is represented using a modified 1.5 level Turbulent Kinetic Energy (TKE) closure and a modified Emanuel moist convection. The UW-NMS explicitly predicts distributions of cloud liquid water, pristine ice, rain, and snow. The UW-NMS has been applied to studies of tropical cloud clusters, hurricanes, midlatitude cyclones, polar lows, and mesoscale convective systems [*Pokrandt et al.*, 1996; *Mecikalski and Tripoli*, 1998; *Avissar et al.*, 1998]. The model has been used to study the impact of synoptic waves on summer column ozone as part of the NASA Polar Ozone Loss over the Arctic Region in Summer (POLARIS) aircraft campaign [*Hitchman et al.*, 1999] and the impact of inertial gravity waves on polar stratospheric clouds as part of the NASA SAGE III Ozone loss and Validation Experiment (SOLVE) campaign [*Hitchman et al.*, 2003]. The UW-NMS can resolve mesoscale deformations of the tropopause associated with cut off lows which can lead to irreversible STE.

[14] For the TRACE-P simulations RAQMS$_G$ extends up to approximately 60 km with a full representation of stratospheric dynamics and chemistry. There are 26 θ-η levels in the vertical: 12 η levels that transition from sigma coordinates at the surface to isentropic coordinates at $\eta_\theta =$ 336 K (near the midlatitude tropopause) and then 14 isentropic layers up to 3300 K (upper stratosphere). Five η layers are below 800 mb. The RAQMS$_N$ domain uses 50 altitude levels with a fixed vertical resolution of 400 m from the surface to 20 km, allowing the influence of STE processes on east Asian tropospheric ozone distributions to be accurately assessed.

[15] The RAQMS global and regional models use an identical chemistry module that includes standard stratospheric odd oxygen (O_x), hydrogen oxide (HO_x), nitrogen oxide (NO_x), chlorine oxide (ClO_x), and bromine oxide (BrO_x) reactions, tropospheric NO_x-HO_x reactions, and oxidation of methane (CH_4) and carbon monoxide (CO). Nonmethane hydrocarbon (NMHC) chemistry is not implemented in the version of the module described here. The chemistry module is based on the LaRC Interactive Modeling Project for Atmospheric Chemistry and Transport (IMPACT) model [*Eckman et al.*, 1995; *Pierce et al.*, 2000; *Al-Saadi et al.*, 2001]. The chemistry computes concentrations for 53 species (Appendix A) using 41 photolytic and 101 gas-phase reactions. Thirty-six chemical families and species are explicitly transported (Appendix A), including total odd oxygen, total odd nitrogen, and total inorganic chlorine and bromine.

[16] Kinetic rates and photolytic quantum yields and absorption cross sections are from *DeMore et al.* [1997] and *Sander et al.* [2000]. The photolytic rates are based on normalized radiative flux functions tabulated as a function of solar zenith angle, overhead column ozone, wavelength, and temperature (S. R. Kawa, personal communication, 1996). For photolysis, a surface albedo of 10% is assumed in the troposphere and a global albedo of 30% is assumed for the stratosphere (to account for underlying tropospheric cloud effects). Surface deposition is computed according to the surface type and drag coefficient, with the calculation of the deposition destruction rate modeled after *Galbally and Roy* [1980] and *Levy et al.* [1985]. Dry deposition is computed for ozone (O_3), peroxides, aldehydes, nitrogen dioxide (NO_2), CO and nitric acid (HNO_3) using deposition velocities from *Müller and Brasseur* [1995]. Rainout is based on first-order rate constants that are fixed in the troposphere. Additionally, heterogeneous loss of nitric pentoxide (N_2O_5) is based on zonal averaged rates from *Dentener and Crutzen* [1993].

[17] An updated CO emission inventory was developed for the TRACE-P simulations [*Kiley et al.*, 2003]. This 1° × 1° source combines global monthly biomass burning CO emissions [*Duncan et al.*, 2002] and global annual industrial emissions derived at Harvard University (J. A. Logan, personal communication, 2002) with 2000 estimates of industrial and biofuel emissions over east Asia [*Streets et al.*, 2003]. Additional global sources of CO in RAQMS include an oceanic source equal to 40 Tg yr^{-1} and estimated sources from isoprene and terpene oxidation based on the Global Emissions Inventory Activity (GEIA) Emission Database for Global Atmospheric Research (EDGAR) database. Production of 2.5 moles of CO per mole of isoprene and 0.8 moles of CO per mole of monoterpenes are assumed. These assumptions result in global CO sources of 585 Tg yr^{-1} from isoprene and 24 Tg yr^{-1} from terpenes. The total global CO emissions are 1571 Tg yr^{-1}. Industrial NO_x emissions are from the 1° × 1° GEIA/EDGAR emission inventory, with east Asian emissions replaced by those from *Streets et al.* [2003]. Aircraft NO_x emissions are obtained from the NASA High Speed Research Program (HSRP) data base [*Stolarski et al.*, 1995] and lightning emissions are distributed according to *Price et al.* [1997] with an annual source of 3 Tg of nitrogen. Monthly NO_x emissions from soils are based on *Yienger and Levy* [1995], as in the GEIA/EDGAR database. Biomass burning emissions of NO_x are scaled to those of CO. The 1° × 1° inventories are mapped onto the grids used within the RAQMS regional and global models. Surface sources of nitrous oxide (N_2O), CH_4, and halocarbons are implicitly assumed by imposing a constant mixing ratio at the surface appropriate for 1990 [*World Meteorological Organization*, 1993].

[18] The RAQMS stratospheric chemistry has been extensively evaluated through comparisons with in situ stratospheric measurements [*Pierce et al.*, 1997, 1999, 2002] and with stratospheric satellite climatologies [*Al-Saadi et al.*, 2001]. For evaluation of tropospheric chemistry, monthly mean chemical climatologies from a multiyear IMPACT model simulation using identical chemistry and emissions databases to RAQMS were examined (not shown). Climatological seasonal variations of ozone at midlatitude ozonesonde stations show good agreement with ozonesonde data throughout the troposphere, but the model underestimates the observed ozone mixing ratios at tropical

ozonesonde stations. Seasonal variations in surface CO are in agreement with climatological data from the National Oceanic and Atmospheric Administration (NOAA) Climate Modeling and Diagnostics Laboratory (CMDL). Additionally, comparisons between climatological altitude profiles of O_3, CO, HNO_3, NO_x, hydrogen peroxide (H_2O_2) and methyl hydroperoxide (CH_3OOH) were compared to composite profiles from various GTE field campaigns (PEM West-A, PEM West-B, PEM Tropics-A, PEM Tropics-B and TRACE-A [*Emmons et al.*, 2000]). The comparisons showed that the IMPACT climatological profiles capture the main features (vertical and latitudinal structure) of the field campaign composites.

3. Method for Estimating STE

[19] The east Asian tropospheric ozone budget during TRACE-P is computed using the RAQMS$_N$ regional domain to define the lateral boundaries of the budget calculations. The tropospheric ozone budget within the RAQMS$_N$ domain is determined by the balance between the following physical processes: horizontal fluxes of ozone through the western, northern, eastern, and southern boundaries of the domain, net in situ tropospheric photochemical production (gross formation-gross destruction), surface deposition, vertical fluxes across the tropopause, and movement of the tropopause. This section outlines the procedure for determining the STE component of the tropospheric ozone budget for east Asia.

[20] Numerous approaches for estimating the flux of mass and trace gases through the tropopause have been developed. *Holton et al.* [1995] provide an overview of these approaches. Most model-based approaches rely on a variant of the generalized formulation discussed by *Wei* [1987] using either a thermal or dynamical definition of the tropopause. *Hoerling et al.* [1993] conducted a global analysis of STE during January using *Wei*'s [1987] isentropic formulation and both dynamical and thermal tropopause definitions. Dynamical and thermal definitions of the tropopause produced similar results although the downward mass flux was somewhat larger across the thermal tropopause than the dynamical tropopause. *Wirth and Egger* [1999] compared 5 methods of diagnosing the synoptic-scale STE including trajectory based estimates (which determine mass flux using kinematic trajectories to define a center of mass for a finite volume), variations of *Wei*'s [1987] general formulation, and a direct approach. They found that *Wei*'s [1987] generalized formula produced different results depending on which coordinate system was used due to near cancellation of large opposing terms. Using potential vorticity (PV) as both a vertical coordinate and tropopause definition provided the most realistic STE for the case considered but required detailed knowledge of the three-dimensional time variation of sources and sinks of PV. A direct method, based on approximating the tropopause using two triangles for each grid box, showed similar grid-scale features as the Wei approach in both pressure and potential temperature.

[21] The proximity of the subtropical jet and associated tropopause break complicates the calculation of STE during TRACE-P for a number of reasons. First, the domain of interest extends from approximately 45°N to the equator
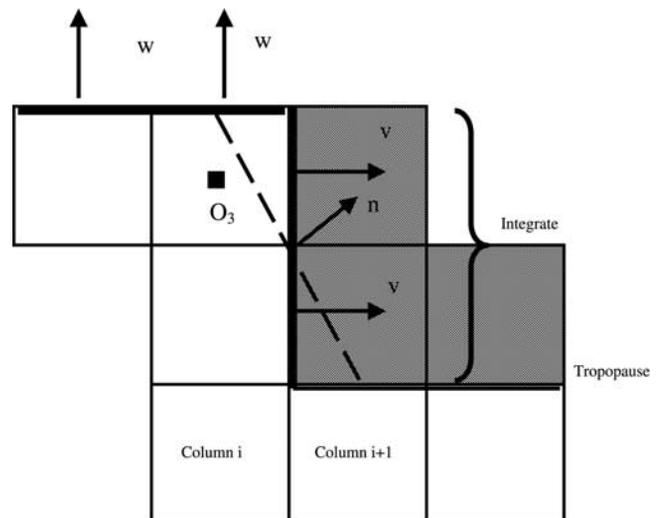

Figure 2. Schematic illustration of the discrete flux calculation.

(Figure 1). Dynamical definitions of the tropopause are only appropriate in midlatitudes. Because of this, we chose the thermal definition of the tropopause for our STE calculations. Second, the tropopause break leads to first-order discontinuities in pressure, altitude and potential temperature on the tropopause. Gradients of these quantities along the tropopause determine the horizontal component of STE in Wei formulations, and sharp discontinuities lead to large numerical errors. Third, mass flux estimates based on trajectory based techniques suffer from the effects of strong shear deformation within the subtropical jet. Initially compact volume elements are elongated along the jet axis, so that the position of a single trajectory cannot be used to define its center of mass. On the basis of these considerations, we have chosen a direct approach for evaluating STE within the RAQMS$_N$ domain. Following *Wirth and Egger* [1999], the cross-tropopause mass flux $F(\rho)$, expressed as a flux per unit horizontal area, is given by

$$F(\rho) = [\rho(\mathbf{u} - \mathbf{c}_{tp})\mathbf{n}]/\cos(\alpha), \quad (1)$$

where ρ is density, $\mathbf{n}$ is the upward normal vector to the tropopause, $\mathbf{u}$ is the three-dimensional velocity vector, $\mathbf{c}_{tp}$ is the vector defining the motion of the tropopause (in direction of unit normal), and α is the angle between $\mathbf{n}$ and the vertical (equation (4) in the work of *Wirth and Egger* [1999]). The magnitude of $\mathbf{c}_{tp}$ is given by

$$|\mathbf{c}_{tp}| = \cos(\alpha)|\delta z^{tp}/\delta t|, \quad (2)$$

where z^{tp} is the altitude of the tropopause. *Wirth and Egger* [1999] defined the local tropopause based on triangles; we consider a discrete thermal tropopause defined by the faces of the RAQMS$_N$ grid boxes and then compute fluxes across those horizontal and vertical faces separating the troposphere from the stratosphere.

[22] Figure 2 is a schematic illustration of the discrete flux calculation. The discrete tropopause (bold line) is represented by a series of stair-step increments. RAQMS$_N$ uses an

Arakawa C grid, consequently O_3 mixing ratios are defined at the center of each box, horizontal velocities are defined on the vertical faces, and vertical velocities are defined on the horizontal faces. The schematic illustrates a case where the tropopause break spans more than one vertical grid box. In these instances, the flux normal to the tropopause surface (indicated by the dashed line), for the grid boxes in column (i) are determined by (1) integrating the zonal and meridional fluxes over the local depth of the tropopause break, (2) projecting this flux onto the horizontal plane, (3) adding the vertical fluxes associated with the upper tropospheric box in column (i), and (4) adding the horizontal projection of the flux associated with the local movement of the tropopause $\mathbf{c}_{tp}$ for the upper tropospheric grid box in column (i).

[23] The horizontal projection of the flux due to the movement of the tropopause is determined by substitution of equation (2) into equation (1) which results in cancellation of the $\cos(\alpha)$ term in the evaluation of the horizontal projection of $\mathbf{c}_{tp}$. The O_3 flux is obtained by multiplying $F(\rho)$ by ozone number density at the discrete tropopause, which is obtained by averaging ozone number densities in adjacent grid boxes.

4.   RAQMS Trace-P Simulations

[24] The RAQMS$_G$ predictions were conducted from 15 February to 15 April 2001 and were constrained with assimilated meteorological data from the European Center for Medium range Weather Forecasting (ECMWF) $1° \times 1°$ analysis. The RAQMS$_N$ prediction was conducted from 7 March to 12 April 2001 using 6 hour meteorological fields from the NOAA National Centers for Environmental Prediction (NCEP) Aviation Model (AVN) $1° \times 1°$ degree analysis for lateral boundary conditions. Meteorological fields from the AVN assimilation were used in the regional simulation because of problems encountered with orographically locked vertical velocities in regional forecasts using ECMWF analyses. These vertical velocities resulted in unrealistic ozone fluxes at the tropopause. Initial chemical conditions for the global simulation were obtained from February monthly means from a multiyear coupled chemical climate run with the LaRC IMPACT model. Initial and boundary conditions for the chemical constituents in regional predictions were obtained from the RAQMS$_G$ prediction.

[25] RAQMS$_G$ was run for a series of 6 hour forecast cycles. At the end of each 6 hour forecast the meteorological variables were reinitialized with ECMWF assimilated fields and the predicted chemical distributions were carried forward. RAQMS$_N$ potential temperature and water vapor predictions were relaxed toward the AVN assimilated fields to provide a weak constraint on the regional meteorological forecasts. These procedures result in on-line global and regional chemical simulations that closely track the synoptic evolution within the assimilated meteorological data sets.

4.1.   Large-Scale Ozone Distribution During Trace-P

[26] This section presents comparisons between the RAQMS predictions and satellite and aircraft remote measurements to demonstrate the model's ability to predict stratospheric and tropospheric ozone distributions over a wide range of spatial and temporal scales. The discussion highlights the multiscale aspects of the RAQMS prediction

and establishes the fidelity of the RAQMS TRACE-P simulations. Figure 3 shows observed and predicted March mean total column ozone, tropospheric column ozone, and composite ozone cross sections. The largest total column ozone amounts (Figure 3 (left)) are found in Northern Hemisphere high latitudes. The Southern Hemisphere shows much lower column ozone. These hemispheric asymmetries are captured in the RAQMS$_G$ column ozone, although the predicted column is overestimated by approximately 50 DU over the North Pole and is lower than TOMS in the tropics. This overestimate at the North Pole and underestimate in the tropics is consistent with an overly strong stratospheric Brewer-Dobson circulation in the ECMWF analysis, a feature found in many data assimilation systems [*Huesmann and Hitchman*, 2003], although the overestimate at the North Pole could also be due to neglecting heterogeneous chemistry associated with polar stratospheric clouds (PSCs) in the TRACE-P simulation. As shown below, the higher observed tropical column ozone could be influenced by tropical tropospheric ozone production due to biomass burning in South America and central Africa during March 2001.

[27] Large-scale upper tropospheric circulation patterns play an important role in determining the longitudinal variations in the altitude of the tropopause and hence column ozone. In regions that are dominated by climatological high-pressure systems, such as over central Asia and the eastern Pacific, the tropopause is elevated and there is a clear latitudinal separation between the high northern latitude and low tropical column ozone. In regions that are dominated by climatological low-pressure systems, such as over the eastern coasts of Asia and North America, the transition from high extra-tropical and low tropical column ozone is very sharp, with column ozone dropping from 450 DU to 250 DU over east Asia near 30°N. The predicted column ozone is in good agreement with the observed distribution in the east Asian region, indicating that the important features of both the large-scale lower-stratospheric ozone transport and tropopause pressures are being accurately predicted within RAQMS$_G$ model. This is critical for the RAQMS predictions of tropospheric ozone formation and destruction during TRACE-P since the sharp gradient in springtime column ozone at 30°N leads to large changes in photolysis rates over east Asia which play a critical role in tropospheric photochemistry in this region [*Crawford et al.*, 1997].

[28] To compare the observed and predicted tropospheric column ozone we use daily TOMS/SBUV derived TOR data from *Fishman et al.* [2003]. We sampled daily RAQMS$_G$ tropospheric column ozone (TCO, analogous to the satellite-derived TOR) at the locations of TOMS/SBUV TOR and then averaged those daily distributions from 1 to 25 March (the last day with TOR estimates). The observed TOR is obtained by subtracting 5 day averaged stratospheric columns derived from empirically corrected SBUV observations from daily TOMS columns [*Fishman et al.*, 2003]. At middle latitudes, 5 day averaging of the SBUV observations leads to smoothing of the lower-stratospheric signatures of tropospheric synoptic disturbances in the column ozone, which often results in aliasing of the synoptic features when subtracted from TOMS. This artifact is similar to one described by *Fishman et al.* [1990] when
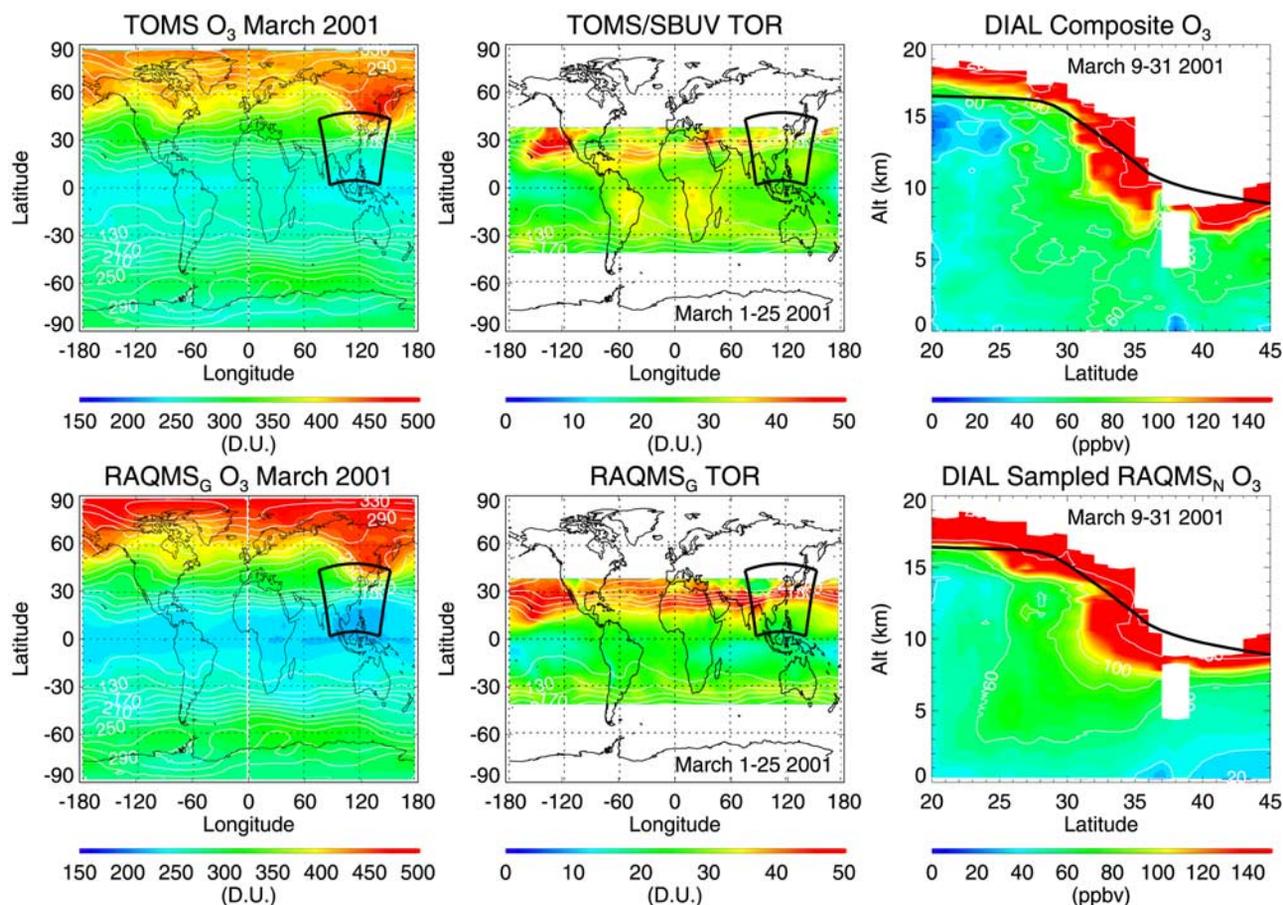
Figure 3. (left) March mean column ozone distributions (colored) from (top) TOMS and (bottom) the RAQMS$_G$ prediction. Bold lines indicate the boundaries of the RAQMS$_R$ domain. The mean pressure of the thermal tropopause, obtained from the UW θ-η model predictions, is contoured in white. (middle) March 2001 (top) monthly mean tropospheric ozone residuals (TOR) and (bottom) the RAQMS$_G$ tropospheric column ozone prediction. (right) Comparisons between composite east Asian tropospheric ozone distributions obtained by (top) the UV DIAL instrument and from (bottom) the RAQMS$_N$ predictions during TRACE-P. The 20, 40, 60, 80, 100, and 200 ppbv ozone mixing ratios are contoured. The mean altitude of the thermal tropopause determined from the UW-NMS prediction is indicated in black.

SAGE (Stratospheric Aerosol and Gas Experiment) data were used with TOMS to calculate the residual. To minimize the effects of this aliasing the objective screening of the TOR data described by *Fishman et al.* [1990] was used except we relaxed the TOR <60 DU restriction to allow for the possibility of higher TOR. We have attempted to assess the degree of synoptic aliasing using a daily noise index defined as the fraction of TOR estimates less than 10 DU within a latitude band. Latitudes with time averaged noise levels greater than 10% were excluded. Points with 1–25 March sampling of less than 66% were also excluded. The observed daily TOR was also filtered in longitude with a 10 point (12.5°) running mean filter to reduce the influence of scan angle-dependent biases in the TOMS data.

[29] Both the observed TOR and predicted TCO distributions (Figure 3 (middle)) are dominated by a 40–50 DU maximum that generally coincides with the Northern Hemisphere subtropical gradient in the tropopause pressure during March 2001. The predicted and observed distributions are in good agreement within the high-pressure circulation in the eastern Pacific, but in general the predicted Northern Hemisphere subtropical TCO is higher than the observed TOR. The predicted east Asian TCO shows a broad maximum extending over the Western Pacific while the observed east Asian TOR is significantly lower. Both observed and predicted TOR fields show a dominant wave-one pattern in the tropical latitudes with a broad minimum over the Pacific basin. This pattern is partially driven by the zonal Walker Circulation with ascending motion associated with convection over Indonesia leading to low tropospheric columns and descending motion over the equatorial Atlantic leading to higher tropospheric columns. However, the observed TOR shows enhanced tropospheric ozone over Brazil and central Africa, presumably associated with biomass burning in this region. These features are absent in the predicted TCO due to the neglect of NMHC chemistry and lack of significant biomass burning emissions in the model's climatological emission data bases during March in these regions. The additional ozone formation associated with biomass burning increases the amplitude of the wave-one

tropical feature in the observed TOR. The predicted band of elevated tropospheric ozone near 30°S is in good agreement with observations.

[30] Figure 3 (right) shows comparisons between east Asian ozone composite cross sections obtained by the Ultra-Violet Differential Absorption Lidar (UV DIAL) instrument [*Browell et al.*, 2003] and RAQMS$_N$ predictions (sampled at the DIAL measurement locations). The RAQMS$_N$ prediction shows evidence of the convective lifting signatures observed in the tropical upper troposphere although the predicted mixing ratios are not as low as observed. This may be due to lateral mixing of high ozone amounts predicted at 25°–30°N near 15 km that are over-estimated in the model. Both observed and predicted tropospheric ozone mixing ratios exceed 100 ppbv below the thermal tropopause from 30° to 45°N, consistent with the predicted high east Asian TCO at these latitudes. Observed and predicted ozone mixing ratios in excess of 60 ppbv extend down from the tropopause to 5 km at 25°N, suggesting that STE plays a significant role in determining the air mass characteristics in this region. DIAL air mass characterization [*Browell et al.*, 2003] indicates that approx-imately 35% of the DIAL ozone observations north of 25°N were associated with stratospheric air. RAQMS$_N$ under-estimates mid tropospheric ozone mixing ratios between 40° and 45°N. However, this latitude band was sampled by only one DC-8 flight (Figure 1).

[31] To quantify the differences between RAQMS ozone predictions and observations we compared longitudinally averaged column ozone distributions. Figure 4 shows the results of these comparisons. Figure 3 (top) shows that the RAQMS$_G$ zonal total mean column ozone is within 10–20 DU of the TOMS observations except poleward of 70°N, where RAQMS$_G$ column ozone is high by as much as 50 DU. Figure 3 (middle) shows that RAQMS$_G$ TCO predictions underestimate the zonal mean observed TOR by 10 DU at 10°S and overestimate the zonal mean observed TOR by 10 DU at 25°N. As discussed above, the model underestimate at southern low latitudes is pri-marily a result of using climatological biomass burning estimates and neglecting NMHC chemistry.

[32] Figure 3 (bottom) shows latitudinal distributions of east Asian TOR from TOMS/SBUV, RAQMS$_G$ TCO, and RAQMS$_N$ TCO averaged between 120° and 150°E (the longitudinal extent of the TRACE-P DC-8 flights), as well as the TCO obtained from the DIAL and DIAL-sampled RAQMS$_N$ composites. The DIAL composite TCO provides an independent measure of the tropospheric column ozone for interpretation of the differences between the RAQMS predictions and TOMS/SBUV observations in E. Asia. Furthermore, comparisons between the RAQMS$_N$ predic-tions averaged between 120° and 150°E and the DIAL-sampled RAQMS$_N$ composite provide a measure of biases introduced in the DIAL composite TCO by the DC-8 flight sampling.

[33] Overall, the east Asian comparisons show that (1) The east Asian RAQMS$_N$, RAQMS$_G$, and TOMS/SBUV TOR are within 5–10 DU of each other in the tropics and subtropics (0°–20°N), (2) The east Asian DIAL-sampled RAQMS$_N$, RAQMS$_G$, and DIAL compos-ite TCO are within 5–10 DU of each other on the equatorward flank of the Japan Jet (20°–30°N) (the high
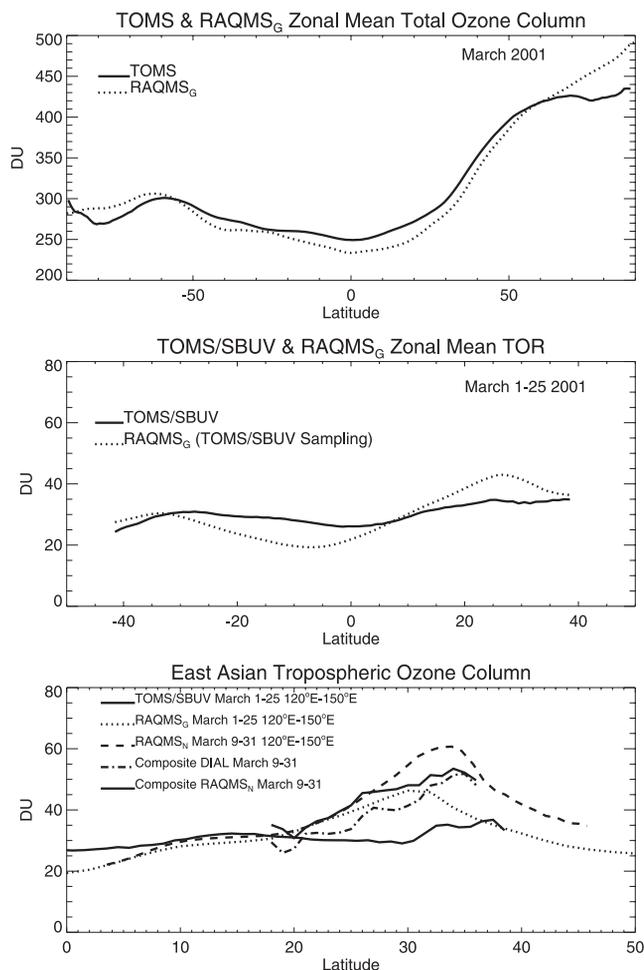

Figure 4. (top) March 2001 zonal mean comparisons between TOMS and RAQMS$_G$ total column ozone. (middle) 1–25 March zonal mean comparisons between TOMS/SBUV and RAQMS$_G$ TOR. (bottom) March 2001 east Asian tropospheric column ozone from TOMS/SBUV, RAQMS$_G$, and RAQMS$_N$ averaged between 120° and 150°E and DIAL and DIAL-sampled RAQMS$_R$ composites for flights between 9 and 31 March 2001.

bias in RAQMS$_N$ is associated with overestimates in ozone mixing ratios just below the tropopause), (3) TOMS/SBUV underestimates the TOR within the Japan Jet (30°N) by 10–15 DU relative to the DIAL composite, (4) The DIAL-sampled RAQMS$_N$ prediction is in good agreement with the DIAL composite on the poleward flank of the Japan Jet (30°–35°N), and (5) Comparison of the DIAL-sampled and RAQMS$_N$ predictions averaged between 120° and 150°E shows that DC-8 flight sampling captures the time averaged TCO except within (±) 4° of the Japan Jet (30°N), where DC-8 sampling underestimates of the time averaged TCO by up to 10 DU.

[34] The RAQMS$_N$ predictions averaged between 120° and 150°E shows time averaged east Asian TCO of 60 DU at 35°N, nearly 20 DU higher than the RAQMS$_G$ predic-tions and 25 DU higher than the TOMS/SBUV TOR at this latitude. The good agreement (differences <5 DU) between the DIAL-sampled RAQMS$_N$ and the DIAL composite TCO at these latitudes provides confidence that the
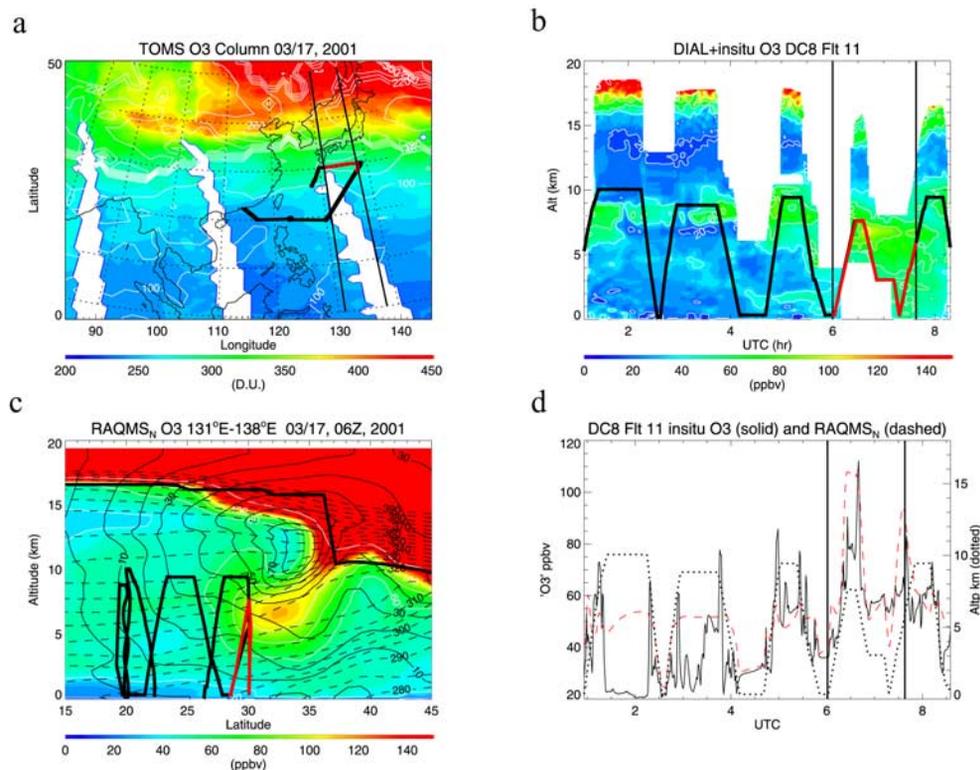
Figure 5. (a) TOMS column ozone for 17 March 2001 within the TRACE-P domain. The black and red line indicates the flight track for DC-8 flight 11. The RAQMS_G 06Z tropopause pressure is shown in white contours. (b) Time series of DIAL ozone measurements for DC-8 flight 11. (c) North–south cross section of ozone mixing ratio averaged between 131° and 138°E at 06Z from the RAQMS_N prediction (this longitude band is indicated by the two black lines extending N–S in Figure 5a). The flight track is indicated in bold lines (with the section of the flight within this cross section indicted by red). Dashed lines indicate isentropes, and the zonal wind within the subtropical jet is contoured. (d) Comparison between the RAQMS_N prediction (dashed line) and in situ (solid line) ozone for DC-8 flight 11. The altitude of the aircraft is indicated by a dotted line.

RAQMS_N TCO prediction is realistic and points to a low bias in both the RAQMS_G TCO and TOMS/SBUV TOR within the Japan Jet. Slightly different averaging periods could account for some of these differences. However, we attribute the low bias in the RAQMS_G prediction primarily to the relatively coarse horizontal resolution ($2° \times 2°$) in the global simulation (the global and regional vertical resolutions are similar in the lower stratosphere).

[35] The inability of the TOMS/SBUV data to capture the increase in TCO within the Japan Jet is most likely related to the algorithm used to extract upper-tropospheric and lower-stratospheric information from the relatively low-vertical-resolution SBUV measurements. The SBUV profile inversion is done in 12 Umkehr layers with the lowest layer (1013-253 mb) nearly 12 km thick. As a result, all of the lowest layer in the SBUV retrieval is assumed to be tropospheric [*Bhartia et al.*, 1996], whereas in reality, some of this layer contains stratospheric air (especially during times of active stratosphere-troposphere exchange) which is not being subtracted from the SBUV total column ozone. The net effect of this assumption is that the resultant stratospheric column ozone (SCO) integral is overestimated. Consequently, when the SCO is subtracted from the concurrent TOMS total ozone measurement, the difference

(TOR) is too low. *Fishman et al.* [2003], developed a procedure that uses the ozonesonde climatology from *Logan* [1999] to empirically correct the SBUV profile in the lowest three Umkehr layers. During this specific case study, this climatology does not capture the high ozone mixing ratios found below the thermal tropopause within the neighborhood of the Japan Jet (see Figure 3), and consequently too much ozone is placed in the stratospheric part of Umkehr layer 2. When the SBUV stratospheric column is subtracted from the TOMS total column, this partitioning leads to the low TOMS/SBUV TOR.

4.2. 17 March 2001 Case Study

[36] It is clear from the previous discussion that the tropopause break and subtropical jet play a significant role in determining the upper tropospheric O_3 distribution off the coast of east Asia. This is illustrated by considering a case study for DC-8 flight 11, which occurred on 17 March 2001. Figure 5a shows the TOMS column ozone, tropopause pressures, and flight track for DC-8 flight 11. The flight originated from Hong Kong, traversed a cold front, and then returned westward before descent into Okinawa, Japan. The tropopause break is evident in the sharp gradient in tropopause pressures near 30°–35°N that extends across

southern Japan. The northernmost leg of the flight track (indicated by thick red line) is the focus of this case study. This flight leg lies near 30°N and extends from 131° to 138°E, roughly parallel to the tropopause break. The tropopause pressure increases (and tropopause altitude decreases) rapidly directly north of this flight segment with tropopause pressures increasing from 140 to 220 mb across the break at these longitudes. TOMS total column ozone ranges from 350 to 450 DU to the north and 250–300 DU to the south of the break.

[37] DIAL ozone measurements (Figure 5b) show that tropospheric ozone mixing ratios are generally between 20 and 40 ppbv except for a thin layer near 8 km with mixing ratios ranging from 40 to 100 ppbv. The tropical tropopause is clearly evident at 17–18 km where ozone mixing ratios increase to >100 ppbv. From 06Z to 08Z (indicated in red along the flight track) the DC-8 encountered a much deeper layer of high ozone mixing ratios (>80 ppbv) near 6 km. A north–south cross section (nearly perpendicular to the flight track) through this feature from the RAQMS$_N$ prediction (Figure 5c) shows that the subtropical jet stream defines an air mass boundary between tropical upper tropospheric air and midlatitude lower-stratospheric air. To the south, ozone mixing ratios are near 40 ppbv in the tropical upper troposphere while to the north ozone mixing ratios are in excess of 100 ppbv in the midlatitude lower stratosphere. The tropopause break extends from 10 to 16 km on the northern flank of the subtropical jet. The mismatch between the thermal and chemical characteristics of the air between the subtropical jet core and the tropopause break results in stratospheric air (from a chemical point of view) below the thermal tropopause. The high ozone within this air mass contributes to the high TCO that RAQMS predicts near 30°N over east Asia (Figure 3). An upper tropospheric front is evident in the vertically compact isentropes below the jet maximum. Ozone mixing ratios in excess of 100 ppbv extend southward from the tropopause break down to 5 km along this upper level front. The high ozone in the DIAL curtain between 06Z and 08Z (this segment of flight track is colored in red) corresponds to the southern extent of this tongue of high ozone. Similar tongues of high ozone were observed on many of the TRACE-P flights and account for the high ozone north of 25°N that is found in the observed and predicted composite cross sections shown in Figure 3. Figure 5d shows a comparison between the RAQMS$_N$ prediction and in situ O$_3$ measurements [*Avery et al.*, 2001]. The DC-8 sampled the layer of elevated ozone on each of the flight legs above 5 km. The model predicts a relatively uniform layer with ozone mixing ratios near 50 ppbv prior to 06Z while in situ measurements show a complex structure within the layer with mixing ratios ranging from 20 to 80 ppbv. The model prediction of mixing ratios within the tongue of high ozone encountered between 06Z and 08Z is in good agreement with the in situ measurements with peak ozone mixing ratios over 100 ppbv and levels above 60 ppbv down to 3 km.

4.3. Statistical Comparison With In Situ Measurements

[38] The preceding discussion demonstrates that the RAQMS predictions are able to reproduce the time averaged ozone distributions observed during TRACE-P and represent the STE transport processes which give rise to a significant portion of the observed ozone distributions in the upper troposphere. However, using RAQMS to diagnose the O$_3$ budget during TRACE-P also requires accurate assessment of the photochemical formation and destruction within the TRACE-P domain. The ability of the RAQMS O$_3$ predictions to capture daily variations in ozone transport, STE and in situ photochemical processes was assessed by statistical comparison with 1 min averaged in situ O$_3$ and NO$_x$ [*Koike et al.*, 2003] from the DC-8 and P-3B aircraft measurements. For a comparison of the RAQMS$_N$ and RAQMS$_G$ CO predictions with in situ measurements and other chemical forecast models that were involved in TRACE-P see *Kiley et al.* [2003]. Additionally, predicted photochemical O$_3$ formation and destruction was compared to that calculated by a detailed photochemical time-dependent box model [*Crawford et al.*, 1999]. The box model calculations also used 1 min averaged data (referred to as the "merged" data set for TRACE-P and available on the GTE TRACE-P public data archive http://www-gte.larc.nasa.gov). Each point was run to diurnal steady state with long-lived species constrained to observations, and daily averaged O$_3$ production and destruction was then computed using the resulting theoretical radical predictions. This comparison includes only the east Asian flights during TRACE-P (DC-8 flights 8–17 and P-3B flights 8–20). RAQMS model results were temporally and spatially interpolated from 6 hour model output to the aircraft flight tracks for direct comparison to the observations and box model output.

[39] Figure 6 shows the results of our statistical analysis. RAQMS$_N$ O$_3$ predictions (Figure 6a) capture the observed median and variability in the 10–12 km altitude range (note that the upper 90% percent have been truncated) but overestimates median ozone mixing ratios and variability between 8 and 4 km. RAQMS$_N$ underestimates the median ozone mixing ratios below 2 km by about 5–10 ppbv. This is consistent with the composite comparisons with DIAL measurements shown in Figure 3.

[40] RAQMS$_N$ is in good agreement with median observed NO$_x$ (Figure 6b) except for a factor of 2 overestimate between 4 and 6 km. Median NO$_x$ in the lowest km is overestimated by RAQMS$_N$ by approximately 20%. RAQMS$_N$ NO$_x$ variability is lower than observed in the free troposphere, due to frequent plume encounters by the P-3B and DC-8 aircraft. High NO$_x$ within the plumes increases the observed variability but cannot be resolved by the 110 km grid used in the regional predictions. Diurnally averaged gross photochemical O$_3$ formation (Figure 6c) and destruction (Figure 6d) are in good general agreement with box model predictions constrained by in situ measurements although the RAQMS$_N$ formation rates are overestimated in the lowest km by nearly 40%. This overestimate of O$_3$ gross formation in the lowest km is consistent with corresponding overestimates of NO$_x$, and reflects the strong dependence of ozone formation on NO$_x$ abundances. Note that although the predicted median gross destruction is in good agreement with box model estimates throughout the troposphere the low RAQMS$_N$ O$_3$ concentrations in the lowest 1 km imply that the gross loss frequency for O$_3$ at this altitude is on the order of 20% higher than the box model.
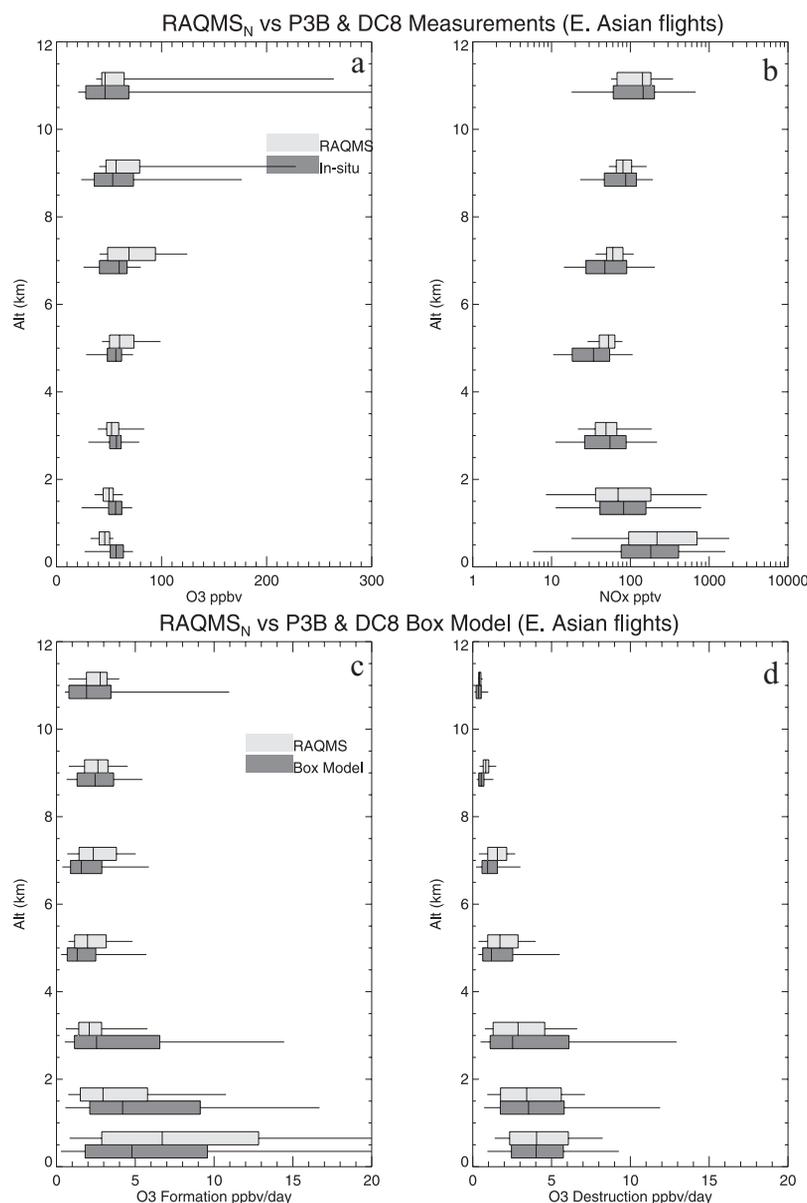
Figure 6. Altitude binned results of statistical analysis of RAQMS$_N$ and in situ measurements. Within each altitude bin, the distributions are characterized by their median, 50th percentile, and 90th percentile (vertical lines, boxes, and horizontal lines, respectively). (a) Results for O$_3$. (b) Results for NO$_x$. (c) Diurnally averaged gross photochemical formation. (d) Destruction of ozone.

[41] RAQMS$_N$ ozone mixing ratios are lower than observed in the lowest 1 km although the predicted median diurnally averaged net ozone production (gross formation-gross destruction) is slightly larger than predicted by the box model. There are several potential explanations for this. One is that surface deposition in RAQMS is too high. As will be shown later, loss due to surface deposition is 37% of the gross formation within the TRACE-P regional domain. Another explanation for the underestimate in ozone within the lowest km is that RAQMS is not simulating vigorous urban O$_3$ production and subsequent transport. *Carmichael et al.* [2003] find that air masses originating from highly industrialized regions of east Asia (Tokyo, Seoul, Shanghai, coastal NE China) were NMHC limited. Urban O$_3$ production, occurring within air parcels prior to sampling by the aircraft, is likely underestimated in the current simulations since RAQMS does not include NMHC chemistry and has horizontal resolution that is too coarse to adequately simulate urban-scale chemistry.

5. RAQMS Estimates of STE

[42] Figure 7 shows the zonal averaged flux of O$_3$ across the tropopause within the RAQMS$_N$ model domain for the period from 7 March to 12 April 2001. The components of the O$_3$ flux and zonal averaged tropopause altitude are also shown. Negatives correspond to fluxes from the stratosphere to the troposphere. The total O$_3$ flux is into the troposphere except for a small flux ($1-2 \times 10^{11}$ mol cm^{-2} s^{-1}) into the stratosphere on the equatorward side of the
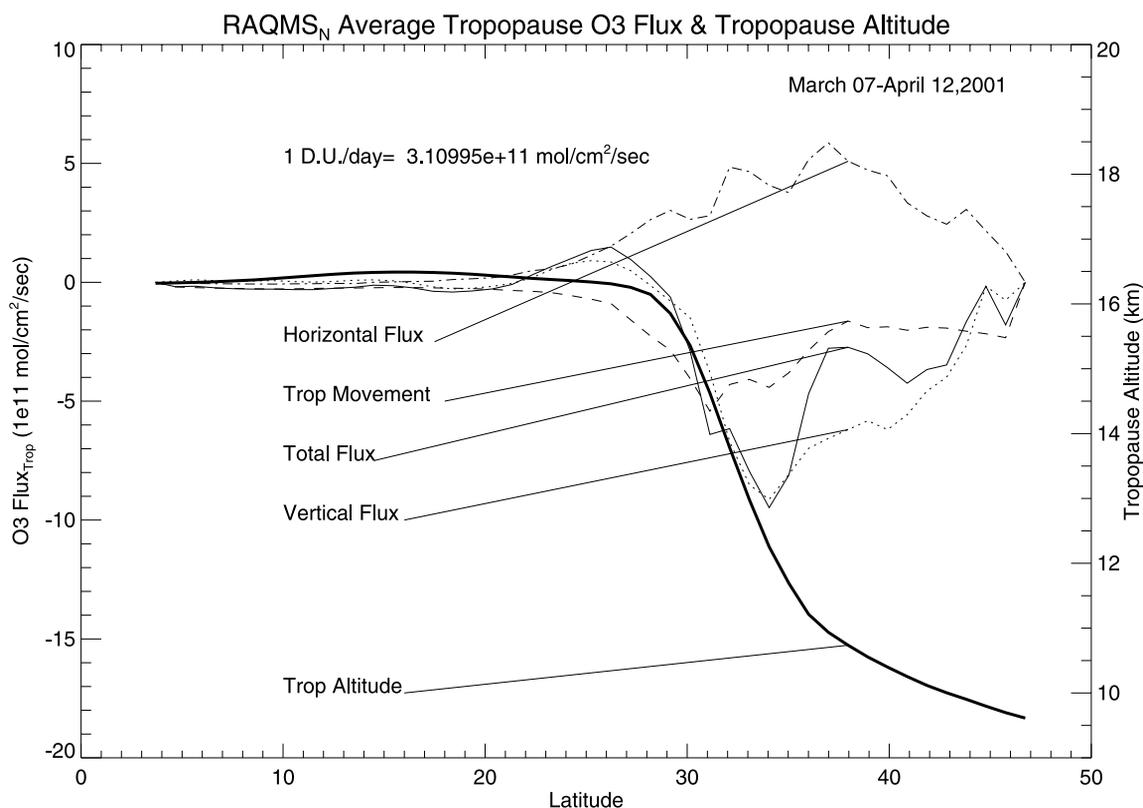
Figure 7. Zonal averaged flux of O_3 across the tropopause within the $RAQMS_N$ model domain for the period from 7 March to 12 April 2001. The components of the O_3 flux and zonal averaged tropopause altitude are also shown.

time averaged tropopause break. The stratosphere to tropo-sphere flux reaches a maximum of -10×10^{11} mol cm^{-2} s^{-1} (3.2 DU d^{-1}) near $30°-35°N$ and is dominated by the vertical flux component. Horizontal fluxes result in net fluxes of ozone from the troposphere to the stratosphere. The movement of the tropopause results in net fluxes from the stratosphere to troposphere. These results are in agree-ment with vertical flux estimates at 7 km over east Asia by *Carmichael et al.* [1998] for the period from 1 to 15 May 1987. They found downward average fluxes of -6.7×10^{11} mol cm^{-2} s^{-1} over the Sea of Japan north of $30°N$ and upward average fluxes of 1.7×10^{11} mol cm^{-2} s^{-1} over the southern part of their east Asian domain (over the Pacific ocean).

[43] The distribution of horizontal and vertical fluxes across the tropopause is consistent with the thermally direct transverse circulation [*Bjerknes*, 1951] in the entrance region of the Japan Jet, located just below the tropopause and to the south of the tropopause break (compare Figure 5). The transverse circulation results in upward motion to the south, poleward motion above, descending motion to the north, and equatorward motion below the jet. Sharp cross-tropopause O_3 gradients above the jet lead to net horizontal and vertical fluxes into the stratosphere in the upper southern quadrant of this circulation. Sharp midlatitude cross-tropopause O_3 gradients lead to vertical fluxes into

the troposphere in the poleward part of the transverse circulation. The daily mean latitude of the tropopause break varies from $30°N$ to $34°N$ within the $RAQMS_N$ domain, but shows little systematic change over the TRACE-P time period. However, the mean altitude of the tropopause north of the tropopause break rises from near 11 km during early March to 12 km by mid-April within the $RAQMS_N$ domain. The rising midlatitude tropopause is in response to seasonal warming of the midlatitude troposphere and leads to fluxes of O_3 from the stratosphere to the troposphere within $RAQMS_N$ domain during the TRACE-P time period.

6. Trace-P O_3 Budgets

[44] The ozone budget for the east Asian region during the TRACE-P mission is estimated by summing instanta-neous estimates of tropopause O_3 fluxes, horizontal O_3 fluxes of on each of the lateral boundaries, 6 hour averaged O_3 gross formation-gross destruction (net production), and 6 hour averaged O_3 surface deposition within the $RAQMS_N$ domain from 7 March to 12 April 2001. Figure 8 shows time average results of these calculations. The time averaged zonal mean O_3 number density for the $RAQMS_N$ domain shows a local maximum of over 110×10^{10} mol cm^{-3} between $20°$ and $30°N$ below 3 km which was not evident in the DIAL sampled $RAQMS_N$ ozone composite shown in
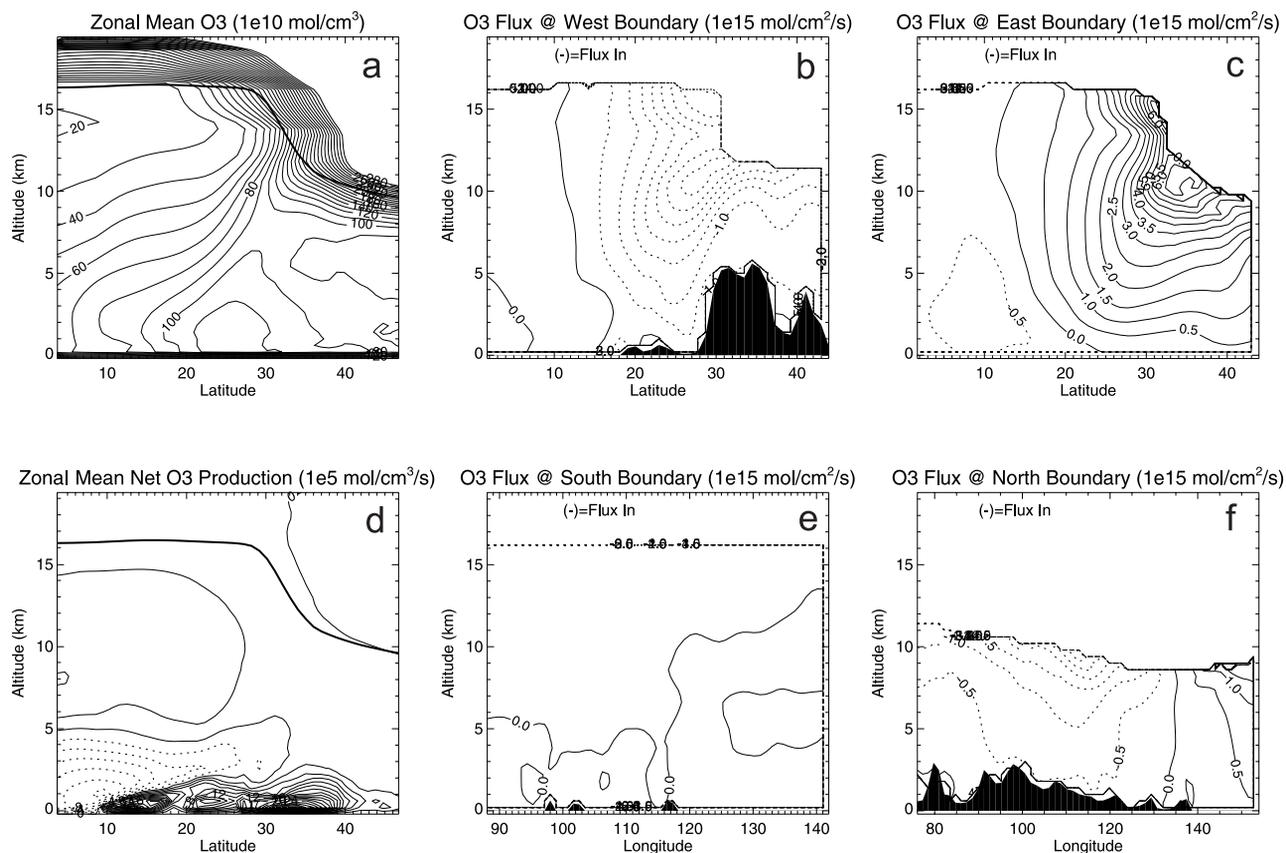
Figure 8. Time-averaged zonal mean O_3 number density (a) within the RAQMS$_N$ domain, horizontal O_3 fluxes on (b) western, (c) eastern, (e) southern, and (f) northern boundaries, and (d) 6 hour averaged net O_3 production from 7 March to 12 April 2001.

Figure 3. These differences arise due to using number density instead of mixing ratio and spatial and temporal sampling by the aircraft. The time averaged zonal mean O_3 production shows net production below 2 km north of 10°N with peaks of 25×10^5 mol cm^{-3} s^{-1} between 10° and 20°N (associated with biomass burning over Thailand) and 33×10^5 mol cm^{-3} s^{-1} at 34°N (associated with industrial emissions from coastal China).

[45] The O_3 flux at the western boundary shows inflow reaching over -3.5×10^{15} mol cm^{-2} s^{-1} near 30°N at both 10 km and 15 km, just to the south of the tropopause break. The Tibetan Plateau defines the lower boundary for the flux calculations north of 30°N. The O_3 flux at the eastern boundary shows maximum outflow in excess of 6.5×10^{15} mol cm^{-2} s^{-1} near 30°N from 10 to 12 km, nearly twice the maximum inflow on the western boundary. This significant increase in O_3 flux is primarily due to the increased upper tropospheric wind speeds on the eastern boundary associated with the core of the Japan Jet (Figure 1). The large difference in the eastern and western fluxes is largely accounted for by net influx from the northern boundary, which shows maximum influx into the domain of over -2.5×10^{15} mol cm^{-2} s^{-1} near 110°E and outflow reaching 1.5×10^{15} mol cm^{-2} s^{-1} (east–west extent of the RAQMS$_N$ domain is 33% larger than the north–south extent). The inflow/outflow pattern on the northern boundary is determined by the location of the planetary-scale trough (Figure 1), evident in the lower tropopause near

140°E, with inflow upstream and outflow downstream of the trough. There are no significant fluxes on the southern boundary of the RAQMS$_N$ domain.

[46] Figure 9 shows time series of spatially integrated contributions from the various components of the O_3 budget. In general, the large horizontal O_3 fluxes shown in Figure 8 tend to balance throughout the TRACE-P time period. Fluxes through the tropopause are predominately negative (into the domain) but there is a high degree of variability at both synoptic (2–3 day) and faster timescales. Surface deposition remains nearly constant due to the use of climatological drag coefficients in the deposition velocity calculations. The net O_3 production reaches up to 1 Tg d^{-1} and shows a strong diurnal cycle with a longer period (~10 day) modulation in peak production.

[47] The total O_3 in the RAQMS$_N$ domain was initially 22.8 Tg. Figure 9c shows a time series of the actual accumulated (instantaneous-initial) O_3 along with the ozone accumulation predicted by our budget calculations (sum of the individual net tendencies). The predicted ozone accumulation when horizontal fluxes, STE or net production is excluded is also shown. The latter three time series illustrate the relative importance of these terms in the overall budget. There is little net change (final-initial) in the amount of ozone in the RAQMS$_N$ domain. The close agreement between the actual accumulated O_3 and the sum of our budget calculations indicates a high degree of accuracy in the budget calculations. The accumulated ozone within the
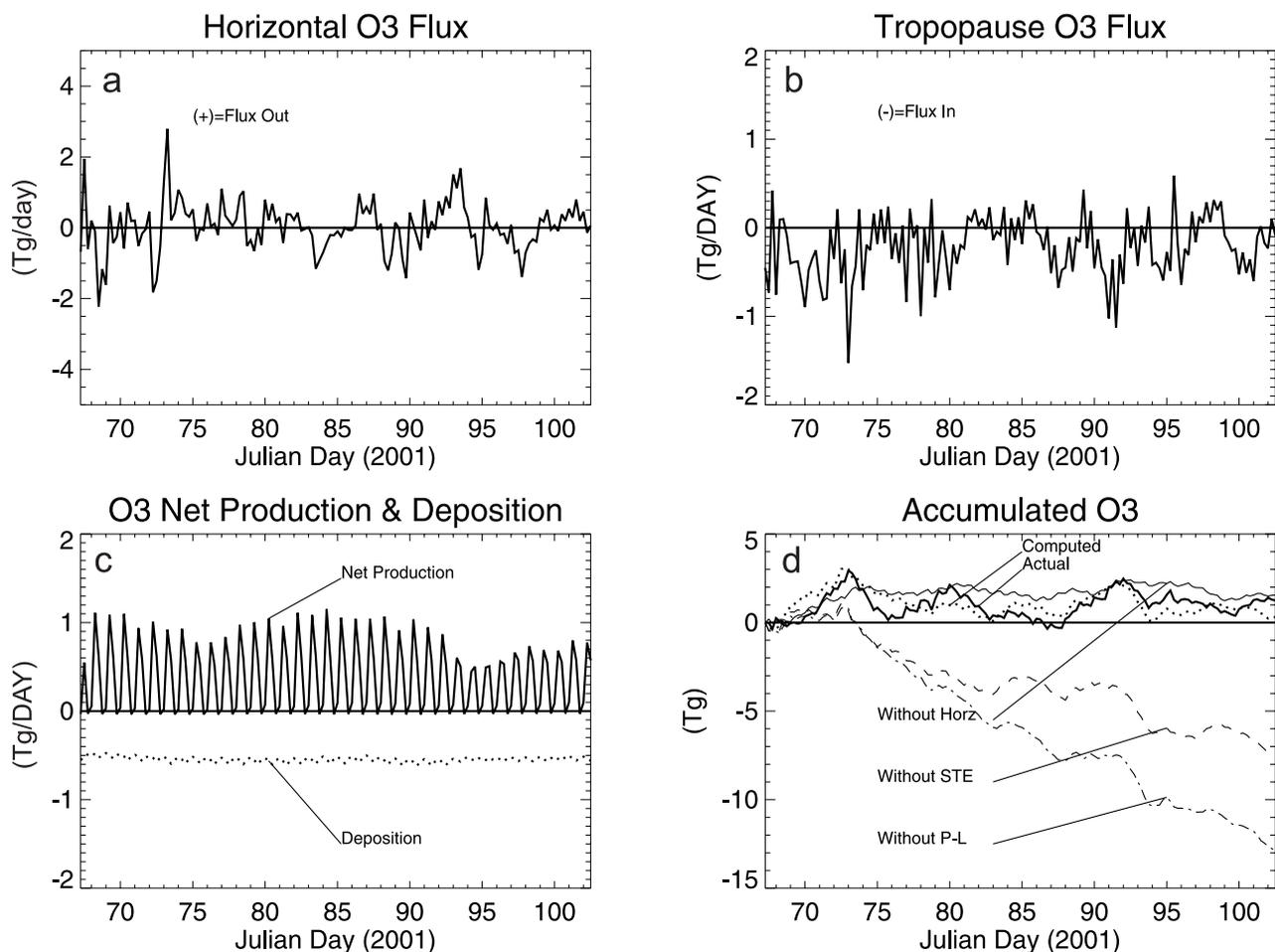
Horizontal O3 Flux

Tropopause O3 Flux

O3 Net Production & Deposition

Accumulated O3

Figure 9.   Time series of spatially integrated O_3 budget terms within the RAQMS$_N$ domain. (a) Sum of the horizontal fluxes. (b) Time series of O_3 fluxes through the tropopause. (c) Time series of net O_3 production (solid line) and deposition (dotted line). (d) Time series of the accumulated (instantaneous-initial) O_3 within the RAQMS$_N$ domain (bold line) along with the ozone accumulation predicted from the sum of the individual net tendencies in our budget calculation (bold dotted line). The predicted ozone accumulation when horizontal fluxes (thin solid line), STE (dashed line), or net production (dash-dotted line) are excluded is also shown to assess the relative importance of these terms in the overall budget.

RAQMS$_N$ domain is generally less than would be the case if the horizontal fluxes were ignored, reflecting net outflow, but neglecting the horizontal fluxes results in very small differences in the accumulated ozone by the end of the time period. On the other hand, neglecting either STE or net photochemical production results in significant declines in the ozone within the RAQMS$_N$ domain. By the end of the TRACE-P time period, STE has contributed 7 Tg, net in situ photochemical production has contributed 13 Tg, and surface deposition (not shown) has destroyed 20.75 Tg of O_3 over east Asia. However, the net photochemical production is itself a balance between gross formation and destruction. Gross formation produces 52 Tg, and gross destruction results in the loss of 39.25 Tg of O_3 over east Asia (not shown).

7.   Discussion and Conclusions

[48] A multiscale modeling system that includes both stratospheric and tropospheric dynamical and chemical processes has been used to evaluate the east Asian ozone budget during TRACE-P. The computed ozone budget explicitly accounts for stratosphere troposphere exchange processes by computing the O_3 flux across a discrete tropopause defined by the model coordinate system. The RAQMS$_G$ total column ozone predictions compare favorably with TOMS measurements and possible reasons for differences between the RAQMS$_G$ TCO and SBUV/TOMS TOR within the TRACE-P domain have been identified. These analyses provide confidence that RAQMS$_G$ predictions can be used as lateral boundary conditions for higher resolution RAQMS$_N$ predictions that focus on the east Asian region. The regional predictions are shown to be in good agreement with remote and in situ O_3 and NO_x measurements collected during TRACE-P. The predicted gross O_3 formation and destruction rates for air masses sampled by the DC-8 and P-3B are consistent with results from box model calculations that are constrained by in situ measurements and include much more detailed treatment of tropospheric chemical processes.

Table 1. Average Ozone Budget Within the RAQMS$_N$ Domain During TRACE-P[a]

Parameter	Value
Average tropopause flux (STE), tg d^{-1}	0.217
Average gross formation (F), tg d^{-1}	1.469
Average gross destruction (D), tg d^{-1}	−1.097
Average surface deposition (Dep), tg d^{-1}	−0.546
Sum of average STE + F + D + Dep, tg d^{-1}	**0.043**
Average western boundary flux, tg d^{-1}	3.493
Average eastern boundary flux, tg d^{-1}	−5.253
Average southern boundary flux, tg d^{-1}	0.073
Average northern boundary flux, tg d^{-1}	1.656
Sum of average boundary fluxes, tg d^{-1}	**−0.030**
Average computed accumulated O$_3$, Tg	1.041
Average actual accumulated O$_3$, Tg	0.966

[a]Positive values indicate a regional increase; negative values indicate a regional decrease. Averages are from 7 March to 12 April 2001.

[49] The overall fidelity of the TRACE-P simulations has allowed us to explicitly evaluate the east Asian tropospheric ozone budget. Table 1 summarizes the average O$_3$ budget during the period from 7 March to 12 April 2001. The average predicted accumulation is 1.04 Tg and the average actual accumulation is 0.966 Tg, indicating an overall accuracy in the budget calculations of 7%. Gross formation (F) dominates STE by a ratio of 7 to 1 in east Asia during TRACE-P. However, this ratio is strongly influenced by the altitude of the tropopause. Sensitivity tests were conducted to examine this dependence. In these tests the instantaneous STE was computed across surfaces defined by the local tropopause minus 2 km and minus 4 km. The STE was reduced by 35% when the tropopause was lowered by 2 km and by 28% when the tropopause was lowered by 4 km. These sensitivity tests indicate that approximately 30% of the ozone advected from the stratosphere across the tropopause over east Asia is subsequently advected out over the Western Pacific within the upper 4 km of the troposphere by the Japan jet.

[50] The average net photochemical production (F − D) within the RAQMS$_N$ domain is 0.37 Tg d^{-1}, or 7% of the average eastward flux (5.25 Tg d^{-1}) during the TRACE-P time period. These results are consistent with *Liu et al.* [2002] who estimate eastward ozone fluxes from Asian fossil fuel and biomass burning account for 9.5% (0.575 Tg d^{-1}) of the total eastward flux (∼6 Tg d^{-1}) between 1000 and 200 mb and 10°–60°N at 150°E during March. However, the present budget analysis implies a very close balance between sources and sinks (STE + F − D − Dep = 0.043 Tg d^{-1}) within the RAQMS$_N$ domain during the TRACE-P time period. This balance results in very small average accumulation (∼1 Tg) of O$_3$ in the east Asian region and very little export averaged over the period (0.03 Tg d^{-1}).

[51] The low ozone export from east Asia predicted by RAQMS$_N$ during TRACE-P is a consequence of relatively high dry deposition rates. RAQMS$_N$ O$_3$ loss due to surface deposition is −0.546 Tg d^{-1}. *Carmichael et al.* [1998] estimate ∼6.5 Tg O$_3$ was removed from their regional model domain during the period from 1 to 15 May 1987, corresponding to an average loss due to dry deposition of −0.433 Tg d^{-1}, or 20% lower than the current deposition rates. The RAQMS$_N$ dry deposition is 37% of the gross formation within the TRACE-P regional domain. This is consistent with the global ozone budget in the IMPACT

model (with identical chemistry), which has globally averaged dry deposition rates of ∼1235 Tg yr^{-1}, or 32% of the globally averaged formation rates. The 1235 Tg yr^{-1} global loss due to dry deposition in the IMPACT model is significantly higher than the 700 ± 300 Tg yr^{-1} quoted by *Lelieveld and Dentener* [2000] but close to the GEOS-CHEM model global deposition of 1070 Tg yr^{-1} [*Bey et al.*, 2001a]. However, both the IMPACT model and RAQMS have larger percentage contributions to the ozone budget from deposition than GEOS-CHEM due to lower gross formation rates. The 37% ratio of surface deposition to gross formation reported here is more than 50% higher than quoted by *Bey et al.* [2001b] who indicate that 21% of ozone produced within their Asian domain is lost to surface deposition, although this comparison is somewhat misleading since our surface deposition includes loss of non-Asian ozone while *Bey et al.* [2001b] are expressing their results relative to Asian ozone. The RAQMS$_N$ ozone budget predictions should be interpreted in light of these considerations. Finally, the influence of urban-scale ozone production on the east Asian ozone budget has not been accounted for in the RAQMS simulations and needs to be explored in more detail. These studies require higher resolution regional simulations and treatment of NMHC chemistry. A second generation RAQMS chemistry module, which includes treatment of NMHC species, has been developed and future studies will explore sensitivities to model resolution and chemical mechanisms.

Appendix A

[52] The chemical constituents used in RAQMS were O$_3$, O, NO, NO$_2$, HNO$_3$, HNO$_2$, NO$_3$, H$_2$O$_2$, OH, HO$_2$, N$_2$O, N$_2$O$_5$, H$_2$O, HCl, CF$_2$Cl$_2$, CFCl$_3$, ClONO$_2$, CH$_4$, CH$_2$O, CO, CH$_3$OOH, CCl$_4$, CH$_3$Cl, Cl, ClO, H, N, O(^{1}D), Cl$_2$, CH$_3$, HCO, CH$_3$O$_2$, CH$_3$O, ClO$_2$, O$_2$, H$_2$, CH$_3$CCl$_3$, HOCl, HO$_2$NO$_2$, Cl$_2$O$_2$, OclO, Br, BrCl, BrO, HBr, HOBr, BrONO$_2$, CH$_3$Br, CF$_3$Br, CF$_2$ClBr, HF, CF$_2$O, and CFClO.

[53] The transported chemical families and species were O$_x$, NO$_y$, HNO$_3$, Cl$_y$, N$_2$O$_5$, H$_2$O$_2$, HCl, ClONO$_2$, OclO, N$_2$O, CFC13 (F11), CF$_2$Cl$_2$ (F12), CCl$_4$, CH$_3$Cl, CH$_3$CCl$_3$ (MTCFM), Br$_y$, CH$_3$Br, CF$_3$Br (H1301), CF$_2$ClBr (H1211), HF, CFClO, CF$_2$O, CH$_4$, HOCl, HO$_2$NO$_2$, H$_2$O (from Met Model), NO$_3$, NO$_2$, CH$_2$O, CO, CH$_3$OOH, HBr, BrONO$_2$, HOBr, BrCl, and Cl$_2$.

References

Al-Saadi, J., R. B. Pierce, T. D. Fairlie, M. M. Kleb, R. S. Eckman, W. L. Grose, M. Natarajan, and J. R. Olson, Response of middle atmosphere chemistry and dynamics to volcanically elevated sulfate aerosol: Three-dimensional coupled model simulations, *J. Geophys. Res.*, 106, 27,255–27,275, 2001.

Avery, M. A., D. J. Westberg, H. E. Fuelberg, R. E. Newell, B. E. Anderson, S. A. Vay, G. W. Sachse, and D. R. Blake, Chemical transport across the ITCZ in hte central Pacific during an El Niño-Southern Oscillation cold phase event in March–April 1999, *J. Geophys. Res*, 106, 32,539–32,553, 2001.

Avissar, R., E. Eloranta, K. Gurer, and G. J. Tripoli, An evaluation of the large eddy simulation option of the Regional Atmospheric Modeling

System in simulating the convective boundary layer: A Fife case study, *J. Atmos. Sci.*, *55*, 1109–1130, 1998.

Bey, I., D. J. Jacob, R. M. Yantosca, J. A. Logan, B. D. Field, A. M. Fiore, Q. Li, H. Y. Liu, L. J. Mickley, and M. G. Schultz, Global modeling of tropospheric chemistry with assimilated meteorology: Model description and evaluation, *J. Geophys. Res.*, *106*, 23,073–23,095, 2001a.

Bey, I., D. J. Jacob, J. A. Logan, and R. M. Yantosca, Asian chemical outflow to the Pacific in spring: Origins, pathways, and budgets, *J. Geophys. Res.*, *106*, 23,097–23,113, 2001b.

Bhartia, P. K., R. D. McPeters, C. L. Mateer, L. E. Flynn, and C. Wellemeyer, Algorithm for the estimation of vertical ozone profiles from the backscattered ultraviolet technique, *J. Geophys. Res.*, *101*, 18,793–18,806, 1996.

Bjerknes, J., Extratropical cyclones, in *Compendium of Meteorology*, edited by T. F. Malone, pp. 577–598, Am. Meteorol. Soc., Boston, Mass., 1951.

Browell, E. V., et al., Large-scale ozone and aerosol distributions, air mass characteristics, and ozone fluxes over the western Pacific Ocean in late winter/early spring, *J. Geophys. Res.*, *108*(D20), 8805, doi:10.1029/2002JD003290, 2003.

Carmichael, G. R., I. Uno, M. J. Phadnis, Y. Zhang, and Y. Sunwoo, Tropospheric ozone production and transport in the springtime in east Asia, *J. Geophys. Res.*, *103*, 10,649–10,671, 1998.

Carmichael, G. R., et al., Regional-scale chemical transport modeling in support of intensive field experiments: Overview and analysis of the TRACE-P observations, *J. Geophys. Res.*, *108*(D21), 8823, doi:10.1029/2002JD003117, in press, 2003.

Carpenter, M. H., A high-order compact numerical algorithm for supersonic flow, in *Twelfth International Conference on Numerical Methods in Fluid Dynamics*, *Lecture Notes in Phys.*, vol. 371, edited by K. W. Morton, pp. 254–258, Springer-Verlag, New York, 1990.

Chen, S. J., Y.-H. Kuo, P.-Z. Zhang, and Q.-F. Bai, Synoptic climatology of cyclogenesis over east Asia, 1958–1987, *Mon. Weather Rev.*, *119*, 1407–1418, 1991.

Colella, P., and P. R. Woodward, The piecewise parabolic method (PPM) for gas-dynamical simulations, *J. Comp. Phys.*, *54*, 174–201, 1984.

Crawford, J., et al., An assessment of ozone photochemistry in the extratropical western North Pacific: Impact of continental outflow during the late winter/early spring, *J. Geophys. Res.*, *102*, 28,469–28,487, 1997.

Crawford, J., et al., Assessment of upper tropospheric HO_x sources over the tropical Pacific based on NASA GTE/PEM data: Net effect on HO_x and other photochemical parameters, *J. Geophys. Res.*, *104*, 16,255–16,273, 1999.

Danielsen, E. F., R. S. Hipskind, S. E. Gaines, G. W. Sachse, G. L. Gregory, and G. F. Hill, Three-dimensional analysis of potential vorticity associated with tropopause folds and observed variations of ozone and carbon monoxide, *J. Geophys. Res.*, *92*, 2103–2111, 1987.

DeMore, W. B., S. P. Sander, D. M. Goldan, R. F. Hampson, M. J. Kurylo, C. J. Howard, A. R. Ravishankara, C. E. Kolb, and M. J. Molina, Chemical kinetics and photochemical data for use in stratospheric modeling, *JPL Publ. 97-4*, eval. 12, 1997.

Dentener, F. J., and P. J. Crutzen, Reaction of N2O5 on tropospheric aerosols: Impact on the global distributions of NO_x, O_3, and OH, *J. Geophys. Res.*, *98*, 7149–7163, 1993.

Duncan, B. N., R. V. Martin, A. C. Staudt, R. Yevich, and J. A. Logan, Interannual and seasonal variability of biomass burning emissions constrained by satellite observations, *J. Geophys. Res.*, *108*(D2), 4100, doi:10.1029/2002JD002378, 2002.

Eckman, R. S., W. L. Grose, R. E. Turner, W. T. Blackshear, J. M. Russell III, L. Froidevaux, J. W. Waters, J. B. Kumer, and A. E. Roche, Stratospheric trace constituents simulated by a three-dimensional general circulation model: Comparison with UARS data, *J. Geophys. Res.*, *100*, 13,951–13,966, 1995.

Emmons, L. K., D. A. Hauglustaine, J.-F. Müller, M. A. Carroll, G. P. Brasseur, D. Brunner, J. Staehelin, V. Thouret, and A. Marenco, Data composites of airborne observations of tropospheric ozone and its precursors, *J. Geophys. Res.*, *105*, 20,497–20,538, 2000.

Fishman, J., Ozone in the troposphere, in *Ozone in the Free Atmosphere*, edited by R. C. Whitten and S. S. Prasad, chap. 4, pp. 161–195, Von Nostrand Reinhold, New York, 1985.

Fishman, J., and P. J. Crutzen, The origin of ozone in the troposphere, *Nature*, *274*, 855–858, 1978.

Fishman, J., C. E. Watson, J. C. Larsen, and J. A. Logan, Distribution of tropospheric ozone determined from satellite data, *J. Geophys. Res.*, *95*, 3599–3617, 1990.

Fishman, J., A. E. Wozniak, and J. K. Creilson, Global distribution of tropospheric ozone from satellite measurements using the empirically corrected tropospheric ozone residual technique: Identification of the regional aspects of air pollution, *Atmos. Chem. Phys. Discuss.*, *3*, 1–24, 2003.

Folkins, I., and C. Appenzeller, Ozone and potential vorticity at the subtropical tropopause break, *J. Geophys. Res.*, *101*, 18,787–18,792, 1996.

Fuelberg, H. E., C. Kiley, J. R. Hannan, D. J. Westberg, M. A. Avery, and R. E. Newell, Meteorological conditions and transport pathways during the transport and chemical evolution over the Pacific (TRACE-P) experiment, *J. Geophys. Res.*, *108*(D20), 8782, doi:10.1029/2002JD003092, in press, 2003.

Galbally, I. E., and C. R. Roy, Destruction of ozone at the Earth's surface, *Q. J. R. Meteorol. Soc.*, *106*, 599–620, 1980.

Hitchman, M. H., M. L. Buker, and G. J. Tripoli, Influence of synoptic waves on column ozone during Arctic summer 1997, *J. Geophys. Res.*, *104*, 26,547–26,564, 1999.

Hitchman, M. H., M. L. Buker, G. J. Tripoli, E. V. Browell, W. B. Grant, T. J. McGee, and J. F. Burris, Nonorographic generation artic polar stratospheric clouds during December 1999, *J. Geophys. Res*, *108*(D5), 8325, doi:10.1029/2001JD001034, 2003.

Hoell, J. M., D. D. Davis, S. C. Liu, R. E. Newell, H. Akimoto, R. J. McNeal, and R. J. Bendura, The Pacific Exploratory Mission-West Phase B: February–March 1994, *J. Geophys. Res.*, *102*, 28,223–28,240, 1997.

Hoerling, M. P., T. K. Schaack, and A. J. Lenzen, A global analysis of stratospheric-tropospheric exchange during northern winter, *Mon. Weather Rev.*, *121*, 162–172, 1993.

Holton, J. R., P. H. Haynes, M. E. McIntyre, A. R. Douglass, R. B. Rood, and L. Pfister, Stratosphere-troposphere exchange, *Rev. Geophys*, *33*, 403–439, 1995.

Holtslag, A. A. M., and B. Boville, Local versus nonlocal boundary-layer diffusion in a global climate model, *J. Clim.*, *6*, 1825–1842, 1993.

Huesmann, A. S., and M. H. Hitchman, The 1978 shift in the NCEP reanalysis stratospheric quasi-biennial oscillation, *Geophys. Res. Lett.*, *30*(2), 1048, doi:10.1029/2002GL016323, 2003.

Jacob, D. J., J. Crawford, M. M. Kleb, V. S. Connors, R. J. Bendura, J. L. Raper, G. W. Sachse, J. Gille, L. Emmons, and J. C. Heald, Transport and Chemical Evolution Over the Pacific (TRACE-P) mission: Design, execution, and first results, *J. Geophys. Res.*, *108*(D20), 8781, doi:10.1029/2002JD003276, 2003.

Jaffe, D., et al., Transport of Asian air pollution to North America, *Geophys. Res. Lett.*, *26*, 711–714, 1999.

Johnson, D. R., T. H. Zapotocny, F. M. Reames, B. J. Wolf, and R. B. Pierce, A comparison of simulated precipitation by hybrid isentropic-sigma and sigma models, *Mon. Weather Rev.*, *121*, 2088–2114, 1993.

Johnson, D. R., A. J. Lenzen, T. H. Zapotocny, and T. K. Schaack, Numerical uncertainties in the simulation of reversible atmospheric processes and entropy conservation, *J. Clim.*, *13*, 3860–3884, 2000.

Johnson, D. R., A. J. Lenzen, T. H. Zapotocny, and T. K. Schaack, Entropy, numerical uncertainties and modeling of atmospheric hydrologic processes: Part B, *J. Clim.*, *15*, 1777–1804, 2002.

Kaneyasu, N., K. Takeuchi, M. Hayashi, S.-I. Fujita, I. Uno, and H. Sasaki, Outflow patterns of pollutants from east Asia to the North Pacific in the winter monsoon, *J. Geophys. Res.*, *105*, 17,361–17,377, 2000.

Kiehl, J. T., J. J. Hack, G. B. Bonan, B. A. Boville, B. P. Briegleb, D. L. Williamson, and P. J. Rasch, Description of the NCAR Community Climate Model (CCM3), *Rep. TN-420+STR*, Natl. Cent. for Atmos. Res., Boulder, Colo., 1996.

Kiehl, J. T., J. J. Hack, G. B. Bonan, B. B. Boville, D. L. Williamson, and P. J. Rasch, The National Center for Atmospheric Research Community Climate Model: CCM3, *J. Clim.*, *11*, 1131–1150, 1998.

Kiley, C., et al., An intercomparison and evaluation of aircraft-derived and simulated CO from seven chemical transport models during the TRACE-P experiment, *J. Geophys. Res.*, *108*(D21), 8819, doi:10.1029/2002JD003089, in press, 2003.

Koike, M., et al., Export of anthropogenic reactive nitrogen and sulfur compounds from the east Asia region in spring, *J. Geophys. Res.*, *108*(D20), 8789, doi:10.1029/2002JD003284, in press, 2003.

Lamarque, J.-F., and P. G. Hess, Cross-tropopause mass exchange and potential vorticity budget in a simulated tropopause folding, *J. Atmos. Sci.*, *51*, 2246–2269, 1994.

Lelieveld, J., and F. J. Dentener, What controls tropospheric ozone?, *J. Geophys. Res.*, *105*, 3531–3551, 2000.

Levy, H., II, J. D. Mahlman, W. J. Moxim, and S. C. Liu, Tropospheric ozone: The role of transport, *J. Geophys. Res.*, *90*(D2), 3753–3772, 1985.

Liu, H., D. J. Jacob, L. Y. Chan, S. J. Oltmans, I. Bey, R. M. Yantosca, J. M. Harris, B. N. Duncan, and R. V. Martin, Sources of tropospheric ozone along the Asian Pacific Rim: An analysis of ozonesonde observations, *J. Geophys. Res.*, *107*(D21), 4573, doi:10.1029/2001JD002005, 2002.

Logan, J. A., An analysis of ozonesonde data for the troposphere: Recommendations for testing three-dimensional models and development of a gridded climatology for tropospheric ozone, *J. Geophys. Res.*, *104*, 16,115–16,149, 1999.

Mecikalski, J. R., and G. J. Tripoli, Inertial available kinetic energy and the dynamics of tropical plume formation, *Mon. Weather Rev.*, 126, 2200– 2216, 1998.

Müller, J.-F., and G. Brasseur, IMAGES: A three-dimensional chemical transport model of the global troposphere, *J. Geophys. Res.*, 100, 16,445–16,490, 1995.

Palmen, E., and C. W. Newton, *Atmospheric Circulation Systems: Their Structure and Physical Interpretation*, *Intl. Geophys. Ser.*, vol. 13, Academic, San Diego, Calif., 1969.

Pierce, R. B., J.-U. Grooss, W. L. Grose, J. M. Russell III, P. J. Crutzen, T. D. Fairlie, and G. Lingenfelser, Photochemical calculations along air mass trajectories during ASHOE/MAESA, *J. Geophys. Res.*, 102, 13,153–13,167, 1997.

Pierce, R. B., J. A. Al-Saadi, T. D. Fairlie, J. R. Olson, R. S. Eckman, W. L. Grose, G. S. Lingenfelser, and J. M. Russell III, Large-scale stratospheric ozone photochemistry and transport during the POLARIS campaign, *J. Geophys. Res.*, 104, 26,525–26,545, 1999.

Pierce, R. B., J. A. Al-Saadi, R. S. Eckman, T. D. Fairlie, W. L. Grose, M. M. Kleb, M. Natarajan, and J. R. Olson, Dynamical climatology of the NASA Langley Research Center Interactive Modeling Project for Atmospheric Chemistry and Transport (IMPACT) model, *J. Geophys. Res.*, 105, 29,109–29,134, 2000.

Pierce, R. B., et al., Large-scale chemical evolution of the Arctic vortex during the 1999/2000 winter: HALOE/POAM III Lagrangian photochemical modeling for the SAGE III—Ozone Loss and Validation Experiment (SOLVE) campaign, *J. Geophys. Res.*, 107(D24), 8317, doi:10.1029/ 2001JD001063, 2002. [printed 108(D5), 2003]

Pokrandt, P. J., G. J. Tripoli, and D. D. Houghton, Processes leading to the formation of mesoscale waves in the midwest cyclone of 15 December 1987, *Mon. Weather Rev.*, 124, 2726–2752, 1996.

Postel, G. A., and M. H. Hitchman, Climatology of Rossby wave breaking along the subtropical tropopause, *J. Atmos. Sci.*, 56, 359–373, 1999.

Price, C., J. Penner, and M. Prather, NO_x from lightning: 2. Constraints from the global atmospheric electric circuit, *J. Geophys. Res.*, 102, 5942–5951, 1997.

Sander, S. P., et al., Chemical kinetics and photochemical data for use in stratospheric modeling, *Rep. 00-3*, suppl. to eval. 12, Jet Propul. Lab., Pasadena, Calif., 2000.

Seo, K.-H., and K. P. Bowman, A climatology of isentropic cross-tropopause exchange, *J. Geophys. Res.*, 106, 28,159–28,172, 2001.

Stolarski, R. S., et al., 1995 scientific assessment of the atmospheric effects of stratospheric aircraft, *Ref. Publ. 1281*, NASA, Washington, D. C., 1995.

Streets, D., et al., An inventory of gaseous and primary aerosol emissions in Asia in the year 2000, *J. Geophys. Res.*, 108(D21), 8809, doi:10.1029/ 2002JD003093, in press, 2003.

Tripoli, G. J., A nonhydrostatic numerical model designed to simulate scale interaction, *Mon. Weather Rev.*, 120, 1342–1359, 1992.

Wang, Y., D. J. Jacob, and J. A. Logan, Global simulation of tropospheric O_3-NO_x-hydrocarbon chemistry: 3. Origin of tropospheric ozone and effects of nonmethane hydrocarbons, *J. Geophys. Res*, 103, 10,757– 10,767, 1998.

Wei, M.-Y., A new formulation of the exchange of mass and trace constituents between the stratosphere and troposphere, *J. Atmos. Sci.*, 44, 3079–3086, 1987.

Wirth, V., and J. Egger, Diagnosing extratropical synoptic-scale stratosphere-troposphere exchange: A case study, *Q. J. R. Meteorol. Soc.*, 125, 635–655, 1999.

World Meteorological Organization, WMO WDCGG data report, *Rep. 4*, 148 pp., http://gaw.kishou.go.jp/wdcgg.html, World Meteorol. Organ. World Data Cent. for Greenhouse Gases, Jpn. Meteorol. Organ., Tokyo, 1993.

Yienger, J. J., and H. Levy II, Empirical model of global soil-biogenic NO_x emissions, *J. Geophys. Res.*, 100, 11,447–11,464, 1995.

Zapotocny, T. H., D. R. Johnson, and F. M. Reames, Development and initial test of the Univ. of Wisconsin global isentropic-sigma model, *Mon. Weather Rev.*, 122, 2160–2178, 1994.

Zapotocny, T. H., A. J. Lenzen, D. R. Johnson, F. M. Reames, P. A. Politowicz, and T. K. Schaack, Joint distributions of potential vorticity and inert trace constituent in CCM2 and UW θ-σ model simulations, *Geophys. Res. Lett.*, 23, 2525–2528, 1996.

Zapotocny, T. H., A. J. Lenzen, D. R. Johnson, F. M. Reames, and T. K. Schaack, A comparison of inert trace constituent transport between the Univ. of Wisconsin isentropic-sigma model and the NCAR Community Climate Model, *Mon. Weather Rev*, 125, 120–142, 1997a.

Zapotocny, T. H., D. R. Johnson, T. K. Schaack, A. J. Lenzen, F. M. Reames, P. A. Politowicz, and Z. Yuan, Simulations of tropospheric joint distributions in the UW θ-σ model and CCM2, *Geophys. Res. Lett.*, 24, 865–868, 1997b.

Zhang, G. J., and N. A. McFarlane, Sensitivity of climate simulations to the parameterization of cumulus convection in the CCC-GCM, *Atmos. Ocean*, 3, 407–446, 1995.

————————————

J. A. Al-Saadi, M. Avery, E. V. Browell, J. Crawford, J. Creilson, T. D. Fairlie, J. Fishman, C. Kittaka, M. Natarajan, J. R. Olson, and R. B. Pierce, NASA Langley Research Center, Mail Stop 401B, Hampton, VA 23681-2199, USA. (j.a.al-saadi@larc.nasa.gov; m.a.avery@larc.nasa.gov; e.v.browell@nasa.gov; j.h.crawford@larc.nasa.gov; j.k.creilson@larc.nasa. gov; t.d.fairle@larc.nasa.gov; j.fishman@larc.nasa.gov; fn.c.kittaka@larc. nasa.gov; m.natarajan@larc.nasa.gov; j.r.olson@larc.nasa.gov; r.b.pierce@ larc.nasa.gov)

M. Buker, M. H. Hitchman, D. Johnson, A. Lenzen, T. Schaack, G. Tripoli, and T. Zapotocny, Space Science and Engineering Center, University of Wisconsin, 1225 W. Dayton Street, Madison, WI 53706, USA. (marcus@dave1.meteor.wisc.edu; matt@aos.wisc.edu; donj@ssec. wisc.edu; allen1@ssec.wisc.edu; todds@ssec.wisc.edu; greg@meteor.wisc. edu; tzap@meteor.wisc.edu)

Y. Kondo, Center for Advanced Science and Technology, University of Tokyo, 4-6-1 Komaba, Meguro-ku, Tokyo 153-8904, Japan. (kondo@ atmos.rcast.u-tokyo.ac.jp)

S. T. Sandholm, Center for Advanced Science and Technology, Georgia Institute of Technology, Baker Building Room 107, Atlanta, GA 30332, USA. (sts@minitower.gtri.gatech.edu)